

Differentiable Invariant Causal Discovery

Yu Wang, An Zhang, Xiang Wang, Yancheng Yuan, Xiangnan He, Tat-Seng Chua

Abstract—Learning causal structure from observational data is a fundamental challenge in machine learning. However, the majority of commonly used differentiable causal discovery methods are non-identifiable, turning this problem into a continuous optimization task prone to data biases. In many real-life situations, data is collected from different environments, in which the functional relations remain consistent across environments, while the distribution of additive noises may vary. This paper proposes Differentiable Invariant Causal Discovery (**DICD**), utilizing the multi-environment information based on a differentiable framework to avoid learning spurious edges and wrong causal directions. Specifically, DICD aims to discover the environment-invariant causation while removing the environment-dependent correlation. We further formulate the constraint that enforces the target structure equation model to maintain optimal across the environments. Theoretical guarantees for the identifiability of proposed DICD are provided under mild conditions with enough environments. Extensive experiments on synthetic and real-world datasets verify that DICD outperforms state-of-the-art causal discovery methods up to 36% in SHD. Our code will be open-sourced.

Index Terms—Causal Discovery, Invariant Learning, Causal Structure Learning, Causal Graph Learning.

1 INTRODUCTION

Causal discovery (CD) is a fundamental problem in a variety of tasks, such as understanding the generation process of data [1], and probing explainability of models [2], [3]. It has tremendous impacts on various domains, like biology [4], [5], and finance [6]. CD aims to learn the causal structure among a set of variables from the observational data and represent the structure as a directed acyclic graph (DAG). The acyclicity constraint frames CD as the combinatorial optimization of discrete edges, which however, is NP-hard. Recently, leading CD solutions [1], [7], [8], [9] gracefully convert the DAG learning into the continuous optimization task. Specifically, the idea stemming from NOTEARS [1] is to build a scoring function upon the adjacency matrix over the variables and find an equivalent continuous constraint on acyclicity.

NOTEARS [1] inspired the development of numerous differentiable causal discovery algorithms that use gradient descent to find the optimal causal graph [10], [11], [12]. When compared to traditional constraint-based causal discovery, these methods have demonstrated superior performance and efficiency in uncovering the true graph with a large amount of data. However, most of them follow the paradigm of empirical risk minimization (ERM) [13] — first imposing the scored DAG on the observations to reconstruct, and then minimizing the empirical risks between the observational and reconstructed data, so as to optimize the DAG. Despite the promising performance, we argue that ERM is prone to capture data biases or shortcut [14], [15], [16], thus derailing the structure learning of DAG. Specifically, the observations of variables are often marred

by some spurious correlations, such as the annotator or selection biases in the data acquisition pipeline [14], thus posing undesired entanglements of variables. ERM easily latches on these correlations [14], [15], [17] to refine the DAG structure, as the following example illustrates.

Consider the ground-truth DAG in Table 1 as the target being reconstructed by the CD solutions, where each edge denotes a causal relationship between two variable nodes. X consists of three variables, which have different relationships with Y : A determines Y , B is influenced by Y , and C is irrelevant to Y . While the CD solutions are designed to identify the causation edges, ERM does not need to learn the correct DAG to reach a low reconstruct loss for fitting the observations. For example, instead of looking at the true causation $B \leftarrow Y$, it is easy to capture the statistical shortcut edge $B \rightarrow Y$, since B is strongly correlated with Y and the reconstructed DAGs achieve even lower losses as compared to the ground-truth DAG. This common problem is consistent with over-reconstruction [18] but remains largely unexplored.

In this study, we aim to design a paradigm that distinguishes the causation edges from spuriously-correlated edges and obtains the faithful DAG. Although learning causal structure from observational data is challenging, we draw inspiration from invariant learning [14], [15], [17] and approximate the task by searching the edges with *invariant* structural equations in multi-environment settings. Across different environments, only factual causation edges remain invariant, while edges with wrong causal directions hardly remain stable, according to the assumptions in *invariant learning* [14]. Though reminiscent of past ideas - e.g., causal structure learning in multi-domain, from heterogeneous/nonstationary data [19], [20], [21], [22], [23], [24], [25] - these methods are only applicable in a linear system or restricted to conditional independence tests, which suffer from high computation complexity as the number of variables increases. To achieve effective differentiable causal discovery in both linear and nonlinear scenarios, we reconsider Table 1 and additionally exhibit the multi-

- Y. Wang, X. Wang and X. He are with University of Science and Technology of China. Email: yuw164@ucsd.edu, xiangwang1223@gmail.com, xiangnanhe@gmail.com.
- A. Zhang, T. Chua are with Sea-NExT Joint Lab from National University of Singapore. Email: an_zhang@nus.edu.sg, dcscts@nus.edu.sg.
- Y. Yuan is with The Hong Kong Polytechnic University. Email: yancheng.yuan@polyu.edu.hk.
- Correspondence to A. Zhang.

TABLE 1

Examples that NOTEARS would find the wrong causal graph while multi-environment settings can help identify the true graph. We present the DAGs derived from minimal reconstruction loss in different environments. The graph on the left denotes the ground truth. The edges in red are wrong or spurious, while the dash one represents the corresponding coefficient is zero. We list the reconstruction loss value following with the triplets in brackets representing coefficients of Y with A , B and C . The loss values and parameters of the potential sub-optimal causal structures learned by NOTEARS in a single environment are highlighted in red. Detailed data generating processes are as follows. $X \sim \mathcal{N}(0, 1)$, $A = X + z_A (\sim \mathcal{N}(0, 1))$, $B = X + Y/2 + z_B^e (\sim \mathcal{N}(0, (\sigma_B^e)^2))$, $C = X/2 + z_C^e (\sim \mathcal{N}(0, (\sigma_C^e)^2))$, $Y = A/4 + \epsilon_Y (\sim \mathcal{N}(0, 1))$. σ_B^e and σ_C^e varies across three environments, e_1, e_2 and e_3 , with $(\sigma_B^e)^2 = (\sigma_C^e)^2 = 1, 2, 4$, respectively.

	e_1	4.57 (0.24, 1.14, -1.32)	5.07 (0.24, 0.32, 0.00)	5.07 (0.24, 0.50, 0.00)
	e_2	6.59 (0.24, 1.09, -1.19)	7.14 (0.24, 0.23, 0.00)	7.07 (0.24, 0.50, 0.00)
	e_3	10.60 (0.24, 1.07, -1.12)	11.21 (0.24, 0.15, 0.00)	11.07 (0.24, 0.50, 0.00)
	e_1	5.05 (0.24, 0.50, 0.10)	4.57 (-0.23, 1.38, -1.54)	5.12 (0.07, 0.29, 0.00)
5.00 (0.25, 0.50, 0.00)	e_2	7.06 (0.24, 0.50, 0.06)	6.59 (-0.24, 1.36, -1.44)	7.17 (0.14, 0.18, 0.00)
7.00 (0.25, 0.50, 0.00)	e_3	11.06 (0.24, 0.50, 0.03)	10.59 (-0.24, 1.35, -1.39)	11.21 (0.18, 0.11, 0.00)
11.00 (0.25, 0.50, 0.00)				

environment information, which impacts the distributions of additive noises. Applying ERM on these environments separately results in different functions when there exist spurious correlations in the causal graph. This inspires us to exclude such unstable edges towards a robust DAG across environments.

Towards this end, we propose **differentiable invariant causal discovery** (DICD), a novel scheme of DAG structure learning that incorporates the idea of invariant learning — that is, learning an invariant DAG with the piece of environment information. Specifically, a DAG generator module learns to generate the environment-aware DAGs from individual environments. For each DAG, the structure equation model (SEM) [26] describes the functions of learned causation edges. We then exploit invariant risk minimization (IRM) [14] to encourage the SEMs to be optimal across all environments, obtaining DAGs regardless of environment changes. On synthetic and real-world datasets, extensive experiments demonstrate the effectiveness of DICD to surpass current state-of-the-art CD solutions.

Our main contributions are:

- To the best of our knowledge, we are among the first class to adopt the environment information into the differentiable causal discovery framework.
- We propose a novel causal discovery solution, DICD, to incorporate invariant learning in both linear and nonlinear settings. Experimental results on synthetic and real-world datasets demonstrate that DICD could significantly better reveal true correlations and eliminate the spurious ones compared to prevalent methods.
- We provide theoretical guarantees for the identifiability of proposed DICD in linear systems under mild conditions, given certain assumptions about the environments.

2 PRELIMINARY

We first make some necessary and reasonable assumptions. Then, we give the task formulation of causal discovery (CD). After that, we introduce the continuous optimization paradigm via empirical risk minimization (ERM), as well as the linear and nonlinear solutions. We list the notations mentioned in our paper in Appendix A

Assumptions. (i) The structural equations are invariant across different environments; (ii) The system is causally sufficient; (iii) Observational data is generated from a structural equation model with independent additive noise; (iv) The distribution shift of additive noise appears in different environments.

The assumptions (i) - (iii) are crucial to our method and provide key insights on how causal structure can be identified from observational data. Assumption (i) states that the invariance principle is held across environments. Assumption (ii) ensures that no hidden confounders exist in the system. In other words, there is no systematic bias induced by hidden confounders. Assumption (iii) implies that only independent additive noise is considered in our paper, which is commonly used in causal discovery. Assumption (iv) defines the multiple environments, which is consistent with the definition of environment assumed in [20], [22] with heterogeneous data [21] or interventional data [19]. A formal definition of different environments is given in Definition 3.1. Technically speaking, assumption (iv) presents both challenges and opportunities for causal discovery and provides a sufficient condition that the causal structure becomes identifiable. A more formal Theorem 4.1 on this argument will be presented later in Section 4.

Task Formulation of CD. Let $\mathbf{X} = [\mathbf{x}_1 | \dots | \mathbf{x}_n]^\top \in \mathbb{R}^{n \times d}$ denote the n observational data of d variables, which are generated from a target directed acyclic graph (DAG). The target DAG is $(\mathcal{V}, \mathcal{D})$, where \mathcal{V} represents the set of node

variables, denoted as $\{X_1, \dots, X_d\}$. And \mathcal{D} is the set of cause-effect edges between variables. The observational data is assumed to be generated from the following SEM:

$$X_j = F_j(Pa(X_j)) + z_j, j \in \{1, \dots, d\}, \quad (1)$$

where X_j is the j -th node variable, F_j is the causal structure function, $Pa(X_j)$ is the set of the parents of X_j , and z_j refers to the additive noise with variance σ_j^2 . Without loss of generality, we assume that the noises are zero-mean. In real-life settings, since the dataset may be obtained from various environments, the distribution of additive noises z_j may differ across different environments. The causal structure functions F_j , on the other hand, are generally invariant. The goal of CD is to learn a DAG to reconstruct the observations \mathbf{X} . The acyclicity restriction of DAG is the fundamental obstacle, because it frames DAG learning as a NP-hard combinatorial optimization task.

Common Paradigm of ERM. Popular differentiable CD solutions, *e.g.*, NOTEARS [1] and its follow-up studies [10], [12], convert DAG learning into a continuous optimization process to overcome the obstacle of the combinatorial optimization problem. The primary idea is to build a scoring function upon the adjacency matrix of variables and discover an equivalent continuous constraint on acyclicity. To optimize the scoring function, they mostly adopt the paradigm of ERM to minimize the empirical risks between the observational and reconstructed data as:

$$\min_f \mathcal{L}(f) = \frac{1}{n} \sum_{i=1}^n l(\mathbf{x}_i, f(\mathbf{x}_i)) \quad \text{s.t. } \mathcal{G}(f) \in \text{DAG},$$

where \mathbf{x}_i is the i -th sample in the dataset. $l(\cdot, \cdot)$ is the reconstruction loss function, *i.e.*, squared loss or negative log-likelihood. $f = (f_1, \dots, f_d)$ formulates the estimated structure function [26] of variables, where $f_i : \mathbb{R}^d \rightarrow \mathbb{R}$ is the estimated structure function of node variable X_i , and thus $f : \mathbb{R}^d \rightarrow \mathbb{R}^d$ is the structure function for all nodes. $f_i(X_1, \dots, X_d)$ is dependent on X_j , if $X_j \in Pa(X_i)$. The score-based solutions seek to learn f conditioning on the DAG constraint: $\mathcal{G}(f) \in \text{DAG}$, where $\mathcal{G}(f)$ refers to the graph corresponding to f .

Following prior studies [1], [10], we use the matrix $\mathbf{W} \in \mathbb{R}^{d \times d}$ to encode the graph $\mathcal{G}(f)$, where each element $[\mathbf{W}]_{ij} \neq 0$ indicates the existence of edge $X_i \rightarrow X_j$. Then we define the matrix \mathbf{W} as:

$$[\mathbf{W}(f)]_{ij} := |\partial_i f_j|, \quad (2)$$

where $\partial_i f_j = \frac{\partial f_j(X_1, \dots, X_d)}{\partial X_i}$ is f_j 's partial derivative *w.r.t.* X_i . Thus, f_j does not depend on X_i if and only if $|\partial_i f_j| = 0$. With Equation (2), we can exploit linear and nonlinear functions f to characterize acyclicity in linear and nonlinear SEMs, respectively.

Linear SEM. In the case of linear SEM [1], we formulate $f(\mathbf{X})$ as a linear matrix multiplication: $f(\mathbf{X}) = \mathbf{X}\mathbf{A}$ (with each instance $f(\mathbf{x}_i) = \mathbf{A}^\top \mathbf{x}_i$, $i \in \{1, \dots, n\}$), where $\mathbf{A} \in \mathbb{R}^{d \times d}$ denotes the coefficient matrix. This formulation frames the acyclicity in Equation (2) as:

$$[\mathbf{W}(f)]_{ij} = |A_{ij}|. \quad (3)$$

Nonlinear SEM. In the case of nonlinear SEM [10], we

define $f_i(\mathbf{X})$ as a multilayer perceptron (MLP) with h hidden layers and an activation function σ as:

$$f_i(\mathbf{X}) = \text{MLP}(\mathbf{X}; \mathbf{A}_i^{(1)}, \dots, \mathbf{A}_i^{(h)}) = \sigma(\dots \sigma(\mathbf{X}\mathbf{A}_i^{(1)}) \dots) \mathbf{A}_i^{(h)}, \quad (4)$$

where $\mathbf{A}_i^{(l)} \in \mathbb{R}^{m_{l-1} \times m_l}$ is the learnable weight matrix of the l -th hidden layer for the i -th node, m_l is the number of hidden units in the l -th layer, and $m_0 = d$. According to [10], we could define $\mathbf{W}_\theta(f)$ as

$$[\mathbf{W}_\theta(f)]_{ij} = \left\| i\text{-th column}(\mathbf{A}_j^{(1)}) \right\|_2. \quad (5)$$

Then the acyclicity constraint could be latched on $\mathbf{W}_\theta(f)$, which serves as the replacement of the intractable $\mathbf{W}(f)$ for nonlinear setting.

3 METHODOLOGY

In this section, we first present differentiable invariant causal discovery (DICD) to conduct causal structural learning over multiple environments. Then, we give detailed formulations in both linear and nonlinear settings.

3.1 Differentiable Invariant Causal Discovery (DICD)

Despite the great success, the ERM paradigm easily captures spurious correlations between variables by over-reconstructing the observations [18] (See the toy example in Table 1). It is essential to distinguish the causation edges from the spuriously-correlated edges. Towards this end, we get access to the multi-environment information and incorporate the idea of invariant learning, so as to frame the causal discovery task as identifying environment-invariant causation edges and discarding environment-dependent correlations.

First, we argue that the multi-environment, in various forms like explicit or implicit metadata, is common in many real-world datasets and can partition the data into different groups or domains. The environments in LFW dataset [27], for instance, can divide the data into black-and-white and colorful photographs. In ImageNet dataset [28], the data can be grouped by different sources and years of images. Moreover, several benchmarks for the domain-shifts problems have been provided by WILDS [29]. Among them, Camelyon17 [30] includes the images collected from five hospitals that serve as different environments, while Amazon [31] provides review texts from different reviewers that can work as environments. Towards the end, the formal definition of the different environments in our paper is given as follow:

Definition 3.1. For two datasets generated from the same structure equation model as shown in Equation (1), if there exists $i \in \{1, \dots, d\}$ such that the distribution of z_i is different across these datasets and X_i is not the source node (see Definition 3.2) in the corresponding graph. Then we say these two datasets are drawn from different environments.

Definition 3.2. We define the node in the graph with no parents as the *Source Node*.

With the environment information, we utilize the invariant learning to conduct multi-environment causal discovery — the function parameters of SEM from the target DAG

should remain optimal across all the environments. Guided by this idea, our DICD consists of two modules: (1) Invariant structural model \mathbf{S} , which presents the structure of DAG, *i.e.*, a binary adjacency matrix. By “invariant”, we mean that \mathbf{S} should be consistent across environments; and (2) Optimal causal function f , which depicts the causal relation of variables. By “optimal”, we mean that f should be optimal over all the environments once the structural model \mathbf{S} is given. Considering the example in Table 1 again, \mathbf{S} is the DAG structure, while f refers to the coefficients of edges. For an invariant DAG structure, completely various optimal coefficients will be learned in different environments. As a result, by utilizing the environment information, incorrect DAGs with smaller reconstruction losses can be excluded based on \mathbf{S} and f .

Having environment-aware groups of observations, we define the empirical risk within the environment $e \in \mathcal{E}$ as:

$$\mathcal{L}^e(\mathbf{S} \circ f) = \frac{1}{n_e} \sum_{i=1}^{n_e} l(\mathbf{X}_i^e, (\mathbf{S} \circ f)(\mathbf{X}_i^e)),$$

where \circ refers to the composition of the two functions, and n_e is the number of samples in environment e . We then build two constraints on \mathbf{S} and f across all environments, and establish the model of DICD:

$$\min_{\mathbf{S} \circ f} \sum_{e \in \mathcal{E}} \mathcal{L}^e(\mathbf{S} \circ f), \quad (6)$$

$$\text{s.t. } \mathcal{G}(\mathbf{S}) = \mathcal{G}(f) \in \text{DAG}, \quad (7)$$

$$f = \arg \min_f \mathcal{L}^e(\mathbf{S} \circ f), \quad \forall e \in \mathcal{E}. \quad (8)$$

Equation (7) states the DAG constraint, where the DAGs represented by \mathbf{S} and f are equivalent. In other words, f latches on \mathbf{S} ’s DAG structure. Equation (8) claims that f refers to the optimal causal model fitting Equation (6) across all environments. Following NOTEARS [10], the DAG constraints can rewrite as hard DAG equation constraints:

$$\mathcal{G}(\mathbf{S}) = \mathcal{G}(f), \quad h(\mathbf{W}(f)) = 0, \quad (9)$$

where $\mathbf{W}(f)$ is defined as Equation (2) in the linear setting and should be replaced with $\mathbf{W}_\theta(f)$ in Equation (5) for the nonlinear setting. Besides $h(\mathbf{W}) = \text{tr}(e^{\mathbf{W} \circ \mathbf{W}}) - d$. Here, \circ refers to the Hadamard product (*aka.* the element-wise product), and $\text{tr}(e^{\mathbf{W} \circ \mathbf{W}})$ is the trace of $e^{\mathbf{W} \circ \mathbf{W}}$.

3.2 Linear SEM

When f characterizes acyclicity in the linear SEM, we have $f(\mathbf{X}) = \mathbf{X}\mathbf{A}$ and $\partial_i f_j(\mathbf{X}) = A_{ij}$ (*cf.* Equation (3)). With the invariant structure model \mathbf{S} as the binary matrix, we can convert $\mathbf{S} \circ f$ as $\mathbf{S} \circ \mathbf{A}$, which is the Hadamard product of \mathbf{S} and \mathbf{A} . However, the bilevel optimization formulation of the DICD model is difficult to solve and is susceptible to failure due to over-parametrization in our setting. We further simplify the learning of these two matrices as the optimization of a new matrix $\mathbf{A}_\mathbf{S} = \mathbf{S} \circ \mathbf{A} \in \mathbb{R}^{d \times d}$. As such, we restrict the loss function in Equation (6) with the DAG constraint in Equation (7) as:

$$\min_{\mathbf{A}_\mathbf{S}} \sum_{e \in \mathcal{E}} \mathcal{L}^e(\mathbf{A}_\mathbf{S}), \quad \text{s.t. } h(\mathbf{A}_\mathbf{S}) = 0.$$

This relaxed version only focuses on optimizing over $\mathbf{A}_\mathbf{S}$ during training. After learning $\mathbf{A}_\mathbf{S}$, we can simply reset coefficient matrix $\mathbf{A} = \mathbf{A}_\mathbf{S}$ and let \mathbf{S} be the binary indicator on $\mathbf{A}_\mathbf{S}$ ’s elements.

We then explore the tractable formulation for the optimality constraint across environments in Equation (8) with the following theorem:

Theorem 3.1. *In the linear setting, we define a matrix variable as $\mathbf{B} \in \mathbb{R}^{d \times d}$. After replacing $\mathbf{S} \circ \mathbf{A}$ with $\mathbf{A}_\mathbf{S}$, the constraint Equation (7-8) satisfy the following necessary condition:*

$$\left\| \frac{\partial \mathcal{L}^e(\mathbf{A}_\mathbf{S} \circ \mathbf{B})}{\partial \mathbf{B}} \Big|_{\mathbf{B}=\mathbf{1}} \right\|_2^2 = 0, \quad \forall e \in \mathcal{E}, \quad (10)$$

where $\mathbf{1}$ is the all-one matrix.

Proof. The basic optimality constraint across environments for Equation (7-8) can be described as:

$$\begin{aligned} \mathbf{A}^* &= \arg \min_{\mathbf{A}} \mathcal{L}^e(\mathbf{S} \circ \mathbf{A}), \quad \forall e \in \mathcal{E}, \\ \text{s.t. } \mathcal{G}(\mathbf{S}) &= \mathcal{G}(\mathbf{A}) \in \text{DAG}. \end{aligned} \quad (11)$$

Then we introduce a new matrix variable \mathbf{B} and insert it into Equation (11). The optimal of \mathbf{B} can be defined as:

$$\mathbf{B}^* = \arg \min_{\mathbf{B}} \mathcal{L}^e(\mathbf{S} \circ \mathbf{A}^* \circ \mathbf{B}), \quad \forall e \in \mathcal{E}. \quad (12)$$

We assert \mathbf{B}^* could be the all-one matrix $\mathbf{1}$, which indicates:

$$\mathcal{L}^e(\mathbf{S} \circ \mathbf{A}^* \circ \mathbf{1}) \leq \mathcal{L}^e(\mathbf{S} \circ \mathbf{A}^* \circ \mathbf{B}), \quad \forall \mathbf{B} \in \mathbb{R}^{D \times D}, \forall e \in \mathcal{E}. \quad (13)$$

Assuming there exists \mathbf{B}' that satisfies $\mathcal{L}^e(\mathbf{S} \circ \mathbf{A}^* \circ \mathbf{B}') < \mathcal{L}^e(\mathbf{S} \circ \mathbf{A}^* \circ \mathbf{1})$, then replacing $\mathbf{A}^* \circ \mathbf{B}'$ with \mathbf{A}' , we could have $\mathcal{L}^e(\mathbf{S} \circ \mathbf{A}') < \mathcal{L}^e(\mathbf{S} \circ \mathbf{A}^*)$. This result obviously contradicts with Equation (11). As such, Equation (13) holds.

We replace $\mathbf{S} \circ \mathbf{A}$ with $\mathbf{A}_\mathbf{S}$. Now if \mathbf{A} is the optimal parameter of Equation (11) (*i.e.*, \mathbf{A}^*), then $\mathbf{A}_\mathbf{S}$ becomes $\mathbf{A}_\mathbf{S}^*$, which yield the following equation:

$$\mathbf{1} = \arg \min_{\mathbf{B}} \mathcal{L}^e(\mathbf{A}_\mathbf{S}^* \circ \mathbf{B}), \quad \forall e \in \mathcal{E}.$$

According to the first-order optimality condition, we have: $\frac{\partial \mathcal{L}^e(\mathbf{A}_\mathbf{S}^* \circ \mathbf{A})}{\partial \mathbf{B}} \Big|_{\mathbf{B}=\mathbf{1}} = \mathbf{0}$. This concludes the proof. \square

Based on Theorem 3.1, we could find that the intractable optimality constraint across environments is now differentiable with the objective Equation (10).

We establish the DICD model in linear cases as follows:

$$\begin{aligned} \min_{\mathbf{A}_\mathbf{S}} \sum_{e \in \mathcal{E}} \mathcal{L}^e(\mathbf{A}_\mathbf{S}) &+ \lambda \sum_{e \in \mathcal{E}} \left\| \frac{\partial \mathcal{L}^e(\mathbf{A}_\mathbf{S} \circ \mathbf{B})}{\partial \mathbf{B}} \Big|_{\mathbf{B}=\mathbf{1}} \right\|_2^2, \\ \text{s.t. } h(\mathbf{A}_\mathbf{S}) &= 0. \end{aligned} \quad (14)$$

This objective function potentially incorporates the invariant structure and the optimal coefficients into the single variable $\mathbf{A}_\mathbf{S}$, thus only adds one more penalty for training compared with NOTEARS.

3.3 Nonlinear SEM

In nonlinear settings, We shall continue to concentrate on the scenario with scalar-valued variables (*i.e.*, $\mathbf{X} \in \mathbb{R}^{n \times d}$) for simplicity. However, the vector-valued variables (*i.e.*, $\mathbf{X} \in \mathbb{R}^{n \times d \times d_x}$) could be simply incorporated into DICD.

NOTEARS-MLP [10] deploys the continuous DAG constraint for nonlinear SEM to the first layer of all the MLPs, as shown in Equation (5). Inspired by this, we establish the relationship between the structure matrix \mathbf{S} and the first layer of the MLPs. In other words, ensuring the parameters of MLP latch on the structure \mathbf{S} in order to satisfy $\mathcal{G}(\mathbf{S}) = \mathcal{G}(f)$ constraint. The precise solution to the equation $\mathcal{G}(\mathbf{S}) = \mathcal{G}(f)$ is to maintain the following restriction throughout the optimization process:

$$\forall i, j, \quad \mathbf{S}_{ji} = 0 \implies \|j\text{-th column}(\mathbf{A}_i^{(1)})\|_2 = 0, \quad (15)$$

where $\mathbf{A}_i^{(1)}$ is the matrix parameter of the first layer in the i -th MLP. The intuition behind the above equation is that setting j -th column($\mathbf{A}_i^{(1)}$) to zero would block the correlation from j to i , corresponding to $\mathbf{S}_{ji} = 0$.

Though the first term in constraint Equation (9) could be formulated in Equation (15). The optimization of Equation (6-8) is still intractable. We need to construct an differentiable term to replace the constraint Equation (15). To address this problem, we propose to simplify the optimization of \mathbf{S} and f to optimizing a new function $f_{\mathbf{S}} = (f_{\mathbf{S}1}, \dots, f_{\mathbf{S}d})$, where $f_{\mathbf{S}i} = \mathbf{S} \circ f_i$. The exact correlation is described in the following equation:

$$\begin{aligned} f_{\mathbf{S}i} &= \mathbf{S} \circ f_i = \text{MLP}(\text{Re}([\mathbf{S}]_i, m_1) \circ \mathbf{A}_i^{(1)}, \mathbf{A}_i^{(2)}, \dots, \mathbf{A}_i^{(h)}) \\ &= \text{MLP}(\mathbf{A}_{\mathbf{S}i}^{(1)}, \mathbf{A}_i^{(2)}, \dots, \mathbf{A}_i^{(h)}), \end{aligned}$$

where m_1 comes from $\mathbf{A}_i^{(1)} \in \mathbb{R}^{m_0 \times m_1}$, and $\text{Re}([\mathbf{S}]_i, m_1)^\top$ refers to $\underbrace{[[\mathbf{S}]_i, \dots, [\mathbf{S}]_i]^\top}_{m_1 \text{ times}}$, with $[\mathbf{S}]_i$ being the i -th column of

\mathbf{S} . We denote $\text{Re}([\mathbf{S}]_i, m_1) \circ \mathbf{A}_i^{(1)}$ as $\mathbf{A}_{\mathbf{S}i}^{(1)}$. Similar to the linear setting, once $f_{\mathbf{S}}$ is learned, we can simply set $f = f_{\mathbf{S}}$ and \mathbf{S} as the adjacency matrix of $\mathcal{G}(f)$. Then f and \mathbf{S} will share the same graph structure. Now we propose the following theorem for nonlinear setting:

Theorem 3.2. *In nonlinear system, we denote $\mathbf{A}_i^{(l)}, l \in \{1, \dots, d\}$ as the parameter of the l -th layer of MLP f_i , and $\mathbf{A}_{\mathbf{S}i}$ is the parameter of the 1st layer of MLP $f_{\mathbf{S}i}$, $i \in \{1, \dots, d\}$. Then after replacing $\text{Re}([\mathbf{S}]_i, m_1) \circ \mathbf{A}_i^{(1)}$ with $\mathbf{A}_{\mathbf{S}i}^{(1)}$, we define a matrix variable as $\mathbf{B} \in \mathbb{R}^{m_1 \times d}$, the optimal condition Equations (7-8) except for the DAG part satisfy the following necessary condition:*

$$\sum_{i=1}^d \left\| \frac{\partial \mathcal{L}^e(\text{MLP}(\mathbf{A}_{\mathbf{S}i}^{(1)} \circ \mathbf{B}, \mathbf{A}_i^{(2)}, \dots, \mathbf{A}_i^{(n)}))}{\partial \mathbf{B}} \right\|_{\mathbf{B}=\mathbf{I}}^2 = 0, \quad \forall e \in \mathcal{E}. \quad (16)$$

Proof. The basic optimal condition described in Equation (7-8) without the DAG constraint could be written as:

$$\begin{aligned} \mathbf{A}_i^{(1)*} &= \arg \min_{\mathbf{A}_i^{(1)}} \mathcal{L}^e(\text{MLP}(\text{Re}([\mathbf{S}]_i, m_1) \circ \mathbf{A}_i^{(1)}, \dots, \mathbf{A}_i^{(n)})), \\ \forall e \in \mathcal{E}, \quad \text{s.t. } \mathcal{G}(\mathbf{S}) &= \mathcal{G}(f), \end{aligned} \quad (17)$$

where $\text{Re}([\mathbf{S}]_i, m_1)$ means $\underbrace{[[\mathbf{S}]_i, \dots, [\mathbf{S}]_i]^\top}_{m_1 \text{ times}}$, with $[\mathbf{S}]_i$ being the i -th column of \mathbf{S} . Note that the following equations with e in this proof indicate all the environments, we omit the condition $\forall e \in \mathcal{E}$ in the following to simplify the proof. Similar to the proof of Proposition 3.1, we define a new matrix $\mathbf{B} \in \mathbb{R}^{m_1 \times d}$, and insert this term into the above equation, then we can have:

$$\mathbf{B}^* = \arg \min_{\mathbf{B}} \mathcal{L}^e(\text{MLP}(\text{Re}([\mathbf{S}]_i, m_1) \circ \mathbf{A}_i^{(1)*} \circ \mathbf{B}, \dots, \mathbf{A}_i^{(n)})). \quad (18)$$

We argue that \mathbf{B}^* could be $\mathbf{1}$, a matrix of dimensions $m_1 \times d$ filled with ones. This is expressed as:

$$\mathbf{1} = \arg \min_{\mathbf{B}} \mathcal{L}^e(\text{MLP}(\text{Re}([\mathbf{S}]_i, m_1) \circ \mathbf{A}_i^{(1)*} \circ \mathbf{B}, \dots, \mathbf{A}_i^{(n)})).$$

Then replacing $\text{Re}([\mathbf{S}]_i, m_1) \circ \mathbf{A}_i^{(1)*}$ with $\mathbf{A}_{\mathbf{S}i}^*$ would yield:

$$\mathbf{1} = \arg \min_{\mathbf{B}} \mathcal{L}^e(\text{MLP}(\mathbf{A}_{\mathbf{S}i}^* \circ \mathbf{B}, \mathbf{A}_i^{(2)}, \dots, \mathbf{A}_i^{(n)})).$$

Again, by the first-order optimality condition, we have Equation (16). \square

With Theorem 3.2, we could transform the intractable constraint in Equation (8) into the differentiable term subject to the first layer of MLP. The detailed formulation in the nonlinear setting can be expressed as:

$$\begin{aligned} \min_{f_{\mathbf{S}}} \sum_{e \in \mathcal{E}} L^e(f_{\mathbf{S}}) \\ + \lambda \sum_{e \in \mathcal{E}} \sum_{i=1}^d \left\| \frac{\partial \mathcal{L}^e(\text{MLP}(\mathbf{A}_{\mathbf{S}i} \circ \mathbf{B}, \mathbf{A}_i^{(2)}, \dots, \mathbf{A}_i^{(n)}))}{\partial \mathbf{B}} \right\|_{\mathbf{B}=\mathbf{I}}^2, \\ \text{s.t. } h(\mathbf{W}_{\theta}(f_{\mathbf{S}})) = 0. \end{aligned} \quad (19)$$

This objective function also potentially uses $f_{\mathbf{S}}$ to both incorporate f and the invariant structure matrix \mathbf{S} .

4 THEORETICAL ANALYSIS

In this section, we aim to provide the sufficient conditions for identifiability of DICD in the linear SEM systems. We will leave the discussion about which assumptions can or cannot be further relaxed in future work.

Theorem 4.1. *For linear SEMs systems with Gaussian additive noises as in Equation (1), if for any $X_i \in \mathcal{V}$ that is not the source node, there exist two environments $e_1, e_2 \in \mathcal{E}$, such that:*

$$\text{Var}(z_i^{e_1}) \neq \text{Var}(z_i^{e_2}), \quad (20)$$

$$\forall X_j \in \mathcal{V} \setminus \{X_i\}, \text{Var}(z_j^{e_1}) = \text{Var}(z_j^{e_2}), \quad (21)$$

where $\text{Var}(\cdot)$ represents the variance, $z_j^{e_1}$ and $z_j^{e_2}$ are the additive noise from $\text{Pa}(X_j)$ to X_j in e_1 and e_2 , respectively. Then the causal structure is **identifiable**.

Here we emphasize that the graph and the coefficients that satisfy the following sufficient conditions and Equation (6-8) will be exactly the true causal graph and the true coefficients, corresponding to the identifiable graph.

Theorem 4.1 indicates that our DICD is guaranteed to retrieve the true causal graph in linear systems, when the diversity of environments is adequate.

The assumptions in Theorem 4.1 are restrictive mainly because Equation (21) requires that the variances of the

nodes other than X_i to be the same across environments e_1 and e_2 . In our proof, Equation (21) is only used for proving Lemma 4.2. However, we will show that, even if we don't assume Equation (21), we may still obtain Equation 32 in the proof of Lemma 4.2 below, which leads to the proof of Lemma 4.2.

With Equation (31), we know the sufficient and necessary condition of $\hat{w}_{j_0}^{e_1} = \hat{w}_{j_0}^{e_2}$ is:

$$\begin{aligned} & \frac{\mathbb{E}_{e_1}[X_i X_{j_0}] - \sum_{k \in Pa_s(i) \setminus \{j_0\}} \hat{w}_k^e \mathbb{E}_{e_1}[X_k X_{j_0}]}{\mathbb{E}_{e_1}[X_{j_0}^2]} \\ &= \frac{\mathbb{E}_{e_2}[X_i X_{j_0}] - \sum_{k \in Pa_s(i) \setminus \{j_0\}} \hat{w}_k^e \mathbb{E}_{e_2}[X_k X_{j_0}]}{\mathbb{E}_{e_2}[X_{j_0}^2]}. \end{aligned}$$

Since we do not have Equation (21), every single term in the above equation is not necessarily equivalent. The probability of the combinations of all these non-equivalent terms being equivalent is very small. Thus during the implementation, Lemma 4.2 is easy to be true. Then the other parts of the proof of Theorem 4.1 will remain the same.

Next, we provide the proof skeleton of Theorem 4.1 and leave the full proof in Appendix A.

There are three main steps in our proof. First, we prove that if the causal structure is correct, then the optimal coefficients are the ground truth coefficients (Lemma 4.1). Second, we show that the stable graph (see definition 4.1) with the minimal sum of reconstruction loss from all environments is exactly the true graph (Theorem 4.2). In the end, we can prove that our algorithm could yield the ground truth graph and coefficients with adequate environments.

To begin with, we give the following lemma to show that our DICD could yield the true coefficient in the linear SEM under the true causal structure.

Lemma 4.1. *Given the true graph G_0 , the corresponding structure S_0 is the adjacency matrix of G_0 . $\forall e \in \mathcal{E}$, we denote the optimal parameters for the coefficients in environment e as:*

$$\hat{W}^e = \arg \min_{\bar{W}} \mathcal{L}^e(S_0 \circ \bar{W}), \quad \text{s.t. } \mathcal{G}(S_0) = \mathcal{G}(\bar{W}). \quad (22)$$

Then we have $\hat{W}^e = W_0, \forall e \in \mathcal{E}$, where W_0 is the ground truth coefficients.

The following definitions are necessary for the rest of this section.

Definition 4.1. For a given graph G , if there exist S, W such that:

$$\begin{aligned} \mathcal{G}(S) &= \mathcal{G}(W) = G, \\ W &= \arg \min_{\bar{W}} \mathcal{L}^e(S \circ \bar{W}), \quad \forall e \in \mathcal{E}, \end{aligned} \quad (23)$$

then we call G a stable graph.

Definition 4.2. For two nodes X_1 and X_2 in a DAG, if X_2 is reachable from X_1 , then X_1 is a predecessor of X_2 . We denote all the predecessors of X_2 in graph G_0 as $Pre_0(X_2)$.

With Definition 4.1, we further denote the parents of the variable X_i in G_0 as $Pa_0(X_i)$ and the corresponding indexes as $Pa_0(i)$. We propose the following Lemma 4.2 to demonstrate that the causal directions between any two variables cannot violate each other in any stable graph

and the true causal graph, which could serve as the pre-conditions in Theorem 4.2 to prove it.

Lemma 4.2. *For any given stable graph G_s , if we assume the conditions in Theorem 4.1 hold, then $\forall X_i \in \mathcal{V}$ which is not a source node, we have $X_i \notin Pre_0(X_j)$ for any $X_j \in Pa_s(X_i)$.*

Finally, Theorem 4.1 can be implied by the following theorem:

Theorem 4.2. *For any given stable graph G_s and the ground truth graph G_0 , we denote their corresponding structures as S_0 and S_s , respectively. We further denote their corresponding consistent optimal parameters as W_s and W_0 , respectively. Then we have:*

$$\sum_{e \in \mathcal{E}} \mathcal{L}^e(S_0 \circ W_0) \leq \sum_{e \in \mathcal{E}} \mathcal{L}^e(S_s \circ W_s), \quad (24)$$

and the equation holds only for $W_0 = W_s$.

The proof of Theorem 4.2 is given in Appendix A. Theorem 4.2 implies that, with the conditions in Equation (7) and Equation (8), The ground truth graph will be yielded by Equation (6).

5 EXPERIMENTS

In this section, we study the empirical performance of our proposed method. We aim to answer the following research questions:

- **RQ1:** How does DICD perform compared to the previous methods in both linear and nonlinear settings?
- **RQ2:** How do DICD and other baselines perform with various factors (*i.e.*, the number of environments, density of graph).
- **RQ3:** How does DICD perform on real-world datasets compared with other applicable baselines?

5.1 Experimental Settings

We now provide the detailed settings for our experiments. The descriptions for the synthetic datasets and the real-world dataset are in Section 5.1.4 and Section 5.1.5, respectively. For all the experiments in this paper, we all generate 10 datasets for each graph setting and report the mean and standard deviation.

5.1.1 Baselines

We select four state-of-the-art causal discovery methods for comparison:

- CD-NOD [21] is a constrained-based causal discovery method designed for heterogeneous datasets, *i.e.*, datasets from different environments. CD-NOD utilizes the independent changes across environments to determine the causal orientations, and proposes constrained-based and kernel-based methods to find the causal structure.
- NOTEARS [1] is specifically designed for linear setting, and is also the backbone of DICD in linear cases. NOTEARS estimates the true causal graph by minimizing the reconstruction loss with the continuous acyclicity constraint. We re-implement NOTEARS with replacing the L-BFGS-B iteration with Adam gradient descent, which

could yield compatible performance and more importantly, could be deployed on GPU.

- NOTEARS-MLP [10] is specifically designed for nonlinear setting, which also serves as the foundation of DICD in nonlinear situations. NOTEARS-MLP approximates the generative SEM model by MLP while only constraining the first layer of the MLP with the continuous acyclicity constraint.
- DAGGNN [7] formulates causal discovery with variational autoencoder, where the encoder and decoder are all graph neural networks. Choosing the evidence lower bound as the loss function and slightly modifying the acyclicity constraint, DAGGNN could manage to recover the weighted adjacency matrix.
- NOCURL [12] utilizes a two-step procedure: first find an initial cyclic solution, then employ Hodge decomposition of graphs and learn an acyclic graph by projecting the cyclic graph to the gradient of a potential function.
- DARING [18] imposes explicit residual independence constraint with an adversarial strategy. We choose the backbone as NOTEARS-MLP to conform with the settings above.

5.1.2 Hyperparameter Settings

For linear settings, there are two hyper-parameters in total: λ_1 for the l_1 -norm regularization term; λ_D for the DICD penalty term. We tune λ_1 in $\{0.01, 0.1\}$ for NOTEARS and DICD. Besides, we tune λ_D in $\{0.1, 1\}$ for DICD. Then for nonlinear settings, there are three hyper-parameters in total: $\lambda_1, \lambda_2, \lambda_D$, among which λ_1 and λ_2 are for the l_1 -norm and l_2 -norm regularization terms, respectively. We tune λ_1, λ_2 both in $\{0.01, 0.1\}$ and λ_D in $\{0.1, 1\}$. The scheduler for λ in Equation (14) and Equation (19) is shown as follows:

$$\lambda = \begin{cases} \frac{k}{K/3} \circ \lambda_D & k \leq K/3 \\ \lambda_D & K/3 \leq k \leq 2K/3 \\ \frac{K-k}{K/3} \circ \lambda_D & k \geq 2K/3 \end{cases},$$

where K is the estimated total step, and k is the current iteration. The intuition behind this scheduler is that we need to let the model fit the data at the beginning, then as the training process goes, we need to enforce our penalty to help find the true causal graph. Then for the last stage, the graph structure has almost been inferred. We need to gradually remove our penalty to let the structural causal function with the given structure fit the data.

5.1.3 Evaluation Protocols

We use the three most popular metrics in causal discovery: false discovery rate (FDR), true positive rate (TPR) and structural Hamming distance (SHD). Higher TPR stand for better performances, while FDR and SHD should be lower to represent the better strategies.

5.1.4 Synthetic Datasets

We conduct experiments on two synthetic datasets for linear and nonlinear settings. Besides, we apply our method DICD on Colored MNIST [32] dataset to explore its effectiveness

on real-world datasets. As for the synthetic data, the ground truth DAG is generated from two random graph models: Erdos-Renyi (ER) and scale-free (SF), following [10]. For the overall experimental comparison, we set the node degree as four. For the linear and nonlinear setting, we construct the environment variable E to simulate the effects of the environments on the additive noises. For the linear setting, after generating the graph, we randomly select $\lfloor 0.3 * d \rfloor$ nodes in this graph, and then build $\lfloor 0.3 * d \rfloor$ new nodes. We call these new variables as the environment variables and denote them as E , and they satisfy the same distributions and are all independent from each other. Then we create $\lfloor 0.3 * d \rfloor$ edges from each environment node to the each selected node. In this way, we could simulate different environments with varying the distribution of the environment variables E .

Then given this new graph with $d + \lfloor 0.3 * d \rfloor$ nodes, we simulate random edge weights to obtain a new matrix $\mathbf{W} \in \mathbb{R}^{(d+\lfloor 0.3*d \rfloor) \times (d+\lfloor 0.3*d \rfloor)}$. With \mathbf{W} , we sample $\mathbf{X} = \mathbf{W}^T \mathbf{X} + \mathbf{z} \in \mathbb{R}^{d+\lfloor 0.3*d \rfloor}$ with \mathbf{z} from Gaussian noise model to generate 10 random datasets $\mathbf{X}_e \in \mathbb{R}^{n \times (d+\lfloor 0.3*d \rfloor)}$. Then we remove the column corresponding to the additional $\lfloor 0.3 * d \rfloor$ environment variables E to generate the final datasets $\mathbf{X} \in \mathbb{R}^{n \times d}$. We change the variances of the noises of the environment variables E to simulate different environments. In the nonlinear setting, after generating the graph, we randomly select $\lfloor 0.5 * d \rfloor$ nodes in the graph, and then create $\lfloor 0.5 * d \rfloor$ environment nodes and also $\lfloor 0.5 * d \rfloor$ edges from each environment node to the selected node. Then given this new graph, we simulate the SEM $\mathbf{X}_j = F_j(\mathbf{X}_{pa(j)}) + \mathbf{z}_j$ for all $j \in \{1 \dots, d + \lfloor 0.5 * d \rfloor\}$ in topological order. For the environment variables, we vary the distributions of the noises in different environments. Then for the other nodes, we set the distribution of the noises as $\mathcal{N}(0, 1)$. We choose f_j to be Additive Noise Models with two-layer MLPs. We will also remove the column corresponding to the variable E to generate the datasets $\mathbf{X} \in \mathbb{R}^{n \times d}$.

5.1.5 Real-world Dataset

For the real-world dataset, We sample 10000 images in total, and 2000 images for each environment. We classify MNIST digits from 2 classes, where classes 0 and 1 indicate original digits (0,1,2,3,4) and (5,6,7,8,9). Then for each environment, we select the ratio of class 0 being green, which is shown in the "Ratio" column in Table 3. Then the noise variances(i.e. noise scale) for each environment are provided in the "Noise Scale" column in Table 3.

5.2 Overall Performances (RQ1)

We present the overall performances of DICD and the baselines for fair comparison. In the baselines, NOTEARS, DAGGNN, NoCurl, DARING are run on the concatenated datasets from all the environments. CD-NOD is run with the environment-id corresponding to each sample.

5.2.1 Linear Synthetic Data

In this experiment, we explore the improvements when introducing different groups by comparing the DAG estimations against the ground truth structure. We simulate {ER4, SF4} graphs with $d = \{10, 20, 50, 100\}$ nodes. For

TABLE 2
Linear Setting, for ER and SF graphs of 10, 20, 50 nodes

ER4	FDR	10 nodes TPR	SHD	FDR	20 nodes TPR	SHD	FDR	50 nodes TPR	SHD
CD-NOD	0.48±0.06	0.17±0.02	33.5±0.9	0.48±0.19	0.11±0.02	75.7±5.0	0.56±0.08	0.15±0.06	195.0±8.0
NOTEARS	0.07±0.01	0.78±0.02	10.1±0.8	0.20±0.03	0.71±0.08	35.9±7.4	0.27±0.04	0.78±0.03	96.7±13.7
DAGGNN	0.08±0.01	0.86±0.02	7.6±0.9	0.34±0.04	0.79±0.05	48.3±7.1	0.36±0.03	0.86±0.03	122.3±14.6
NOCURL	0.14±0.01	0.81±0.01	9.8±0.4	0.19±0.02	0.92±0.01	22.3±2.4	0.31±0.02	0.94±0.01	89.5±9.5
DARING	0.08±0.01	0.81±0.03	9.3±1.3	0.38±0.07	0.58±0.07	60.9±9.9	0.48±0.01	0.60±0.06	187.6±4.9
DICD	0.03±0.01	0.88±0.02	4.9±1.0	0.16±0.03	0.89±0.04	19.7±5.8	0.26±0.02	0.89±0.06	82.0±5.3
SF4	FDR	TPR	SHD	FDR	TPR	SHD	FDR	TPR	SHD
CD-NOD	0.36±0.10	0.19±0.02	25.0±1.4	0.34±0.05	0.18±0.01	59.3±0.9	0.38±0.04	0.15±0.01	168.3±1.7
NOTEARS	0.04±0.04	0.81±0.02	6.1±1.1	0.19±0.01	0.77±0.02	27.1±1.5	0.17±0.01	0.83±0.01	60.7±2.5
DAGGNN	0.07±0.03	0.98±0.02	2.9±1.5	0.27±0.03	0.84±0.02	31.6±2.6	0.26±0.02	0.88±0.01	80.6±8.3
NOCURL	0.06±0.02	0.86±0.02	4.8±1.1	0.25±0.01	0.86±0.01	28.2±1.3	0.26±0.08	0.93±0.05	71.8±10.6
DARING	0.17±0.04	0.86±0.07	9.0±2.7	0.26±0.02	0.80±0.01	32.6±1.8	0.28±0.02	0.87±0.01	87.3±5.9
DICD	0.05±0.04	0.98±0.02	2.3±1.7	0.16±0.05	0.81±0.09	22.1±8.4	0.18±0.03	0.91±0.01	53.7±8.7

TABLE 3
Experimental Settings for Colored MNIST.

Environment	Ratio	Noise Scale
e_1	0.16	10/255
e_2	0.32	20/255
e_3	0.48	30/255
e_4	0.64	40/255
e_5	0.80	50/255

each environment, we generate 200 samples. We evaluate our methods with datasets from 5 environments, and the variances of Gaussian noise for the environment variable E in each environment are $\{0.2, 0.4, 0.6, 0.8, 1.0\}$. Table 2 and Table 6 summarizes the results when the number of nodes equals to $\{10, 20, 50, 100\}$. From these tables, we could have the following key observations: (1) DICD has outperformed all other baselines across various settings. More precisely, DICD achieves significant improvements over the strongest baselines by up to 36% in SHD (10 nodes, ER graph). (2) Generally, DICD has the lower FDR and higher TPR, which also coincides with the intuition that DICD could eliminate spurious correlations and reveal the true ones.

5.2.2 Nonlinear Synthetic Data

We also conduct enormous experiments to demonstrate the effectiveness of DICD in the nonlinear setting. Similarly to the linear setting, we simulate $\{\text{ER4}, \text{SF4}\}$ graphs with $d = \{10, 20, 50, 100\}$ nodes. For each graph, we generate data from two environments, 1000 samples for each environment. The Gaussian noises for the environment variable E in these two groups are $\{0.2, 0.4\}$. The results with $d = \{10, 20, 50\}$ are provided in Table 4 and results with $d = 100$ are shown in Table 7. From these tables, we could find: (1) DICD consistently outperforms other baselines in all eight settings upon the most crucial metric SHD. The improvements on SHD over the best baseline are up to 29% (50 nodes, ER graph). (2) DICD achieves compatible FDR with NOTEARS but far higher TPR. This shows that in the nonlinear setting, DICD is better at revealing the true causal correlations that might have been missed by NOTEARS. (3)

The over-reconstruction problem still exists in other methods, while DICD has the potential to mitigate it, which could be the reason for the performance improvements. (4) CD-NOD performs fairly well in nonlinear cases, which means the multi-environment setting might be more helpful when the correlations between variables are more complicated. However, CD-NOD consumes in average more than 9 hours in the simplest setting (10 nodes), and more than 300 hours in the case of 50 nodes, which is far more expensive than our algorithm. As shown in Table 5, we only record the running time of CD-NOD in nonlinear settings, since its running time is almost unacceptable in these cases. Then we report the averaged running time for different seeds and different graph types (ER or SF). From the table, we can observe that CD-NOD is very expensive for nonlinear cases, while the running time of DICD almost remain constant when the number of nodes get larger.

5.3 Study of Various Factors (RQ2)

In this section, we discuss various factors that may affect the performances of DICD and other methods. Due to limit of space, we discuss the effect of environmental imbalance in Appendix 5.3.2.

5.3.1 The Effect of Environment Number

To explore how the number of environments affects the performances, we conduct experiments on both linear and nonlinear settings. The total number of the examples is set to 1000. We choose $d = 10$ and $s_0 = 40$ with ER graph for this case study. If the number of the environments is N , then the number of samples for each environment is $\lfloor 1000/N \rfloor$. The noises for different environments are sliced from the head of the array $\{0.2, 0.4, 0.6, 0.8, 1.0, 0.1, 0.3, 0.5, 0.7, 0.9\}$. For example, the noises are $\{0.2, 0.4\}$ when the number of environments is 2. In Figure 1, we can observe: (1) When the number of environments is greater than 4 in the linear setup, more environments will not yield to better results, which means for simple structure equation models, four environments may have already ruled out the possibility of incorrect graphs. (2) In the nonlinear setting, it is amazing to

TABLE 4
Nonlinear Setting, for ER and SF graphs of 10, 20, 50 nodes

ER4	FDR	10 nodes TPR	SHD	FDR	20 nodes TPR	SHD	FDR	50 nodes TPR	SHD
CD-NOD	0.39±0.06	0.50±0.07	20.0±3.1	0.31±0.04	0.56±0.06	56.8±4.2	0.35±0.07	0.82±0.05	115.7±18.3
NOTEARS-MLP	0.24±0.10	0.44±0.12	23.8±3.5	0.25±0.05	0.35±0.09	59.0±5.0	0.30±0.08	0.86±0.06	102.9±25.4
DAGGNN	0.50±0.06	0.21±0.04	32.2±1.5	0.61±0.07	0.24±0.05	82.9±4.5	0.62±0.06	0.15±0.03	217.0±16.0
NOCURL	0.38±0.02	0.38±0.05	27.4±1.5	0.56±0.07	0.34±0.07	80.2±7.6	0.69±0.07	0.28±0.07	258.2±25.2
DARING	0.44±0.04	0.28±0.04	29.8±2.7	0.55±0.09	0.23±0.07	77.6±5.7	0.58±0.09	0.23±0.05	209.4±20.0
DICD	0.20±0.08	0.57±0.10	19.2±4.3	0.26±0.06	0.69±0.07	40.3±6.1	0.26±0.04	0.88±0.03	84.4±11.7

SF4	FDR	TPR	SHD	FDR	TPR	SHD	FDR	TPR	SHD
CD-NOD	0.42±0.03	0.68±0.04	19.5±2.5	0.31±0.09	0.64±0.07	46.3±6.8	0.32±0.05	0.75±0.09	104.3±12.1
NOTEARS-MLP	0.41±0.10	0.31±0.16	25.2±4.6	0.29±0.10	0.56±0.10	51.0±7.4	0.29±0.08	0.72±0.13	113.7±17.3
DAGGNN	0.62±0.09	0.26±0.07	31.2±3.4	0.69±0.07	0.16±0.03	80.1±7.4	0.64±0.03	0.15±0.05	210.3±8.2
NOCURL	0.54±0.06	0.40±0.10	26.2±2.0	0.70±0.04	0.27±0.05	87.2±3.0	0.70±0.02	0.22±0.01	240.8±9.3
DARING	0.54±0.10	0.27±0.05	29.0±2.7	0.58±0.06	0.21±0.03	73.1±4.5	0.53±0.03	0.19±0.02	193.0±5.0
DICD	0.34±0.06	0.71±0.15	16.2±4.3	0.27±0.06	0.68±0.15	37.9±7.1	0.29±0.04	0.80±0.03	99.3±9.0

TABLE 5
Running time comparison

	10 nodes	20 nodes	50 nodes
CD-NOD	>9h	>64h	>300h
DICD	15min	15min	15min

TABLE 6
Linear Setting, for ER and SF graphs of 100 nodes

Method	FDR	ER4 TPR	SHD	FDR	SF4 TPR	SHD
NOTEARS	0.17±0.03	0.78±0.03	147.9±15.7	0.12±0.04	0.91±0.02	81.4±23.0
DAGGNN	0.23±0.03	0.79±0.04	178.3±9.6	0.31±0.02	0.92±0.01	195.3±20.4
NOCURL	0.25±0.01	0.94±0.00	136.0±5.3	0.14±0.04	0.98±0.01	69.8±23.2
DARING	0.29±0.02	0.69±0.04	234.0±14.3	0.29±0.01	0.90±0.01	180.9±5.4
DICD	0.20±0.03	0.87±0.01	133.9±16.2	0.12±0.03	0.97±0.01	61.9±15.6

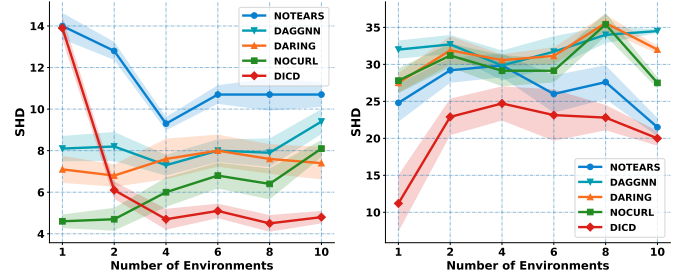
TABLE 7
Nonlinear Setting, for ER and SF graphs of 100 nodes

Method	FDR	ER4 TPR	SHD	FDR	SF4 TPR	SHD
NOTEARS	0.20±0.04	0.40±0.07	270.0±24.1	0.17±0.06	0.42±0.10	260.1±27.3
DAGGNN	0.52±0.05	0.09±0.01	390.6±7.7	0.50±0.08	0.09±0.02	390.3±13.4
DARING	0.41±0.05	0.15±0.02	367.0±8.8	0.42±0.04	0.15±0.02	367.3±6.9
NOCURL	0.62±0.06	0.23±0.02	447.2±33.0	0.60±0.03	0.18±0.02	418.6±10.7
DICD	0.18±0.05	0.54±0.10	226.6±23.1	0.18±0.03	0.53±0.06	228.0±16.3

find that DICD could achieve better performance even there is only one environment. The reason could be that when there are more parameters in the function, the explicit constraint on the optimality of the parameters could contribute much to learning the best graph, which is more likely to be the ground truth graph. (3) More environments in nonlinear settings could degrade the performance of all approaches; the reason for this could be that heterogeneous noises can be particularly unfriendly when the relationships between variables become quite intricate.

5.3.2 The Effect of the Imbalance between Different Environments

Since the imbalance of data is the major problem in machine learning, we aim to explore how the imbalance of data size between different environments would affect the



(a) Linear Setting (b) Nonlinear Setting
Fig. 1. SHD w.r.t. the number of environments.

performances of our method and other baselines. The total number of samples in this dataset is 1000 for linear settings and 2000 for nonlinear settings. We choose ER graphs with $d = 20$ and $s_0 = 4d = 80$ for this case study. The noises for the variable E in two environments are set to be $\{0.2, 0.4\}$. Then the ratio in Figure 2 means the percentage of the samples from the first environment. From this figure, we could have the following observations: (1) In most of the settings, DICD outperforms other methods consistently, except when the data is higher imbalanced in linear setting, where there is almost only one environment. (2) In both linear and nonlinear settings, the balanced situation is the best for DICD, which means we have enough information from every environment. (3) Even there is only one group, DICD could make significant improvements against NOTEARS, which coincides with the discovery in Section 5.3.1.

5.3.3 The Effect of Density of Graph

We aim to discover how much the node degree (*i.e.*, density) will affect our algorithm compared to the other baselines. We choose SF graph with $d = 20$ for this case study. In the linear setting, we generate samples from five environments, 200 samples for each. And for nonlinear settings, we draw samples from two environments, 1000 samples for each. The x-axis represents the mean degree of the nodes in the generated graph. For instance, Node degree = 10 means there are 200 edges in total when generating the SF graph. From Figure 4, we could observe: (1) DICD almost

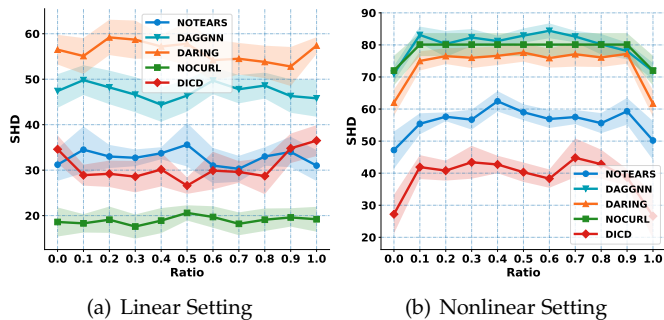


Fig. 2. SHD for different percentage of imbalance between two environments in linear and nonlinear settings.

consistently outperforms the other methods, except for few cases. (2) As the node degree (*i.e.*, the density) increases, especially in nonlinear settings, the improvements of DICD over baselines get larger, which means DICD could better adapt to the denser settings.

5.4 Real Data (RQ3)

Finally, we evaluate our method on the real-world data: ColoredMNIST. Our method, as well as NOTEARS-MLP, could be simply extended to the setting of vector-valued variable. DAG-GNN is already designed to work in this situation. However, DARING do not discuss this situation in the paper. Though it seems that DARING could also be generalized to vector-valued, efforts need to be taken. Thus we omit it as comparison in this section. As stated earlier in Section 5.1.5, we sample 10000 images from the MNIST dataset and generate the colored version of MNIST. In the pictures, we have kept the digits to be black, while the background has the color red or green. The images are resized to 8*8, and then flattened to yield a 64-dim vector. The label vector and color vector are set to be all zeros or all ones (according to the original label) with dimension as 64. Then during searching (or training) we only consider the possible correlations among the white backgrounds, colors, noises, and digits. Thus we have four variables in the designed task. As shown in Figure 3. We could find NOTEARS, DAGGNN and NoCurl all make mistakes, while DICD gives reasonable predictions.

6 RELATED WORK

Causal Discovery has caught enormous attention recently. We will mainly discuss the differentiable score-based algorithms and the works considering multi-environments.

Differentiable Score-based algorithms. Score-based causal discovery methods aim to find the causal structure by optimizing a carefully defined score function via various modelling methods. Though there are conventional methods [33], [34], [35], [36], [37] applying various techniques such as hill-climbing [38] and integer programming [39], the differentiable methods using gradient descent show stronger power. NOTEARS [1] reformulate the causal discovery problem with acyclicity constraint as a continuous program. DAG-GNN [7] proposes a variant of the acyclicity constraint and solves the generalized linear SEM in a graph

autoencoder structure. NOTEARS-MLP [10] and GRANDAG [9] extend the continuous acyclicity regularization into a neural network and achieve better results in the nonlinear settings. RL-BIC [8] introduces RL to find the DAG with the best BIC score. DARING [18] proposes to constrain the independence between the residuals and adopts an adversarial training strategy. DAG-GAN [40] formulates the problem of DAG structure learning from the perspective of distributional optimization. [41] shows that applying soft sparsity and DAG constraints would be enough. There are also other works that apply some alternatives of the continuous acyclicity regularization. DAG-NOFEAR [42] propose the constraint term that only depends on the absolute value of the adjacency matrix \mathbf{W} , instead of $\mathbf{W} \odot \mathbf{W}$ in $h(\mathbf{W})$ in Equation (9), which is correlated to l_1 penalty and sparsity. NOCURL [12] aims at eliminating the DAG constraint entirely, by showing that the set of weighted adjacency matrices of DAGs are equivalent to the set of weighted gradients of graph potential functions. NODAG [43] proposes to solve an l_1 -penalized optimization, while ENCO [44] provides convergence guarantees without constraining the score function with respect to acyclicity. These methods all have their own strategies to control the acyclicity.

Previous work considering multi-environments. Most work with multi-environment settings are built on constraint-based methods [21], [45], [46], [47], [48]. Although they achieved lots of improvements, there are some major limitations: 1) may have overly strict domain definition [19]; 2) limited to linear cases only [20], [22], [23]; 3) designed to solve much simpler problems than CD such as causal direction identification [23], [24]; 4) may involve a large number of independence tests and be very time-consuming [20], [21], which is also the general problem of constrain-based methods. However, We define the environments following [14], [20], [22], and our method is capable of solving the general causal discovery problems in both linear and nonlinear cases. There is another interesting and more general task called Federated Causal Discovery [49], [50], [51], [52], [53], which aims to solve the problem about decentralized datasets. Though our targets are different, the algorithms are somewhat similar.

7 CONCLUSION AND FUTURE WORK

Despite the great success in causal structure learning, today's differentiable causal discovery methods are still suffering from non-identifiability issue and over-reconstruction problem from observation data. Utilizing the inherent heterogeneity when environment partition is provided in advanced is not yet discussed in the differentiable causal discovery task. In this paper, we proposed a simple yet effective Differentiable Invariant Causal Discovery (DICD) method to tackle the challenge by incorporating the multi-environment information. Our main idea is that, given the true causal graph, the parameters of SEM learned from different environments should remain consistent. Theoretical guarantees for the identifiability of proposed DICD are provided under certain assumptions about the environments. The extensive experimental results demonstrate the effectiveness of DICD.

One limitation of DICD is the requirement of prior knowledge of the environment. In the future study, we will

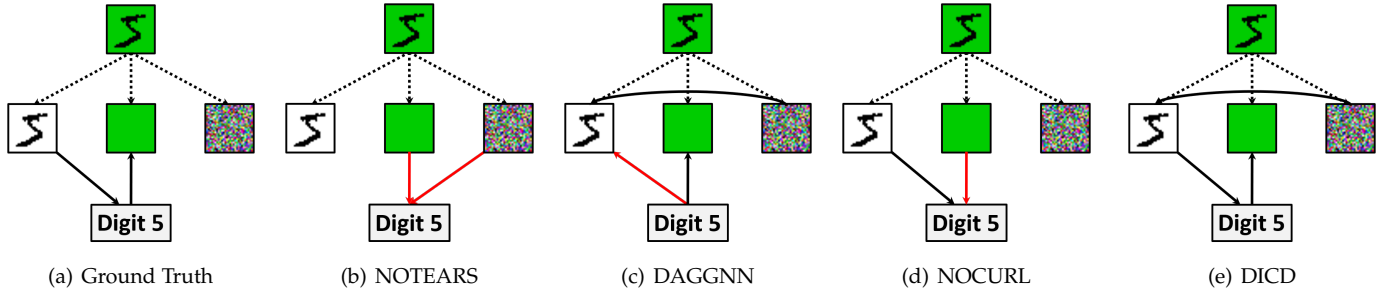


Fig. 3. Revealed graph by different methods on Real World Data

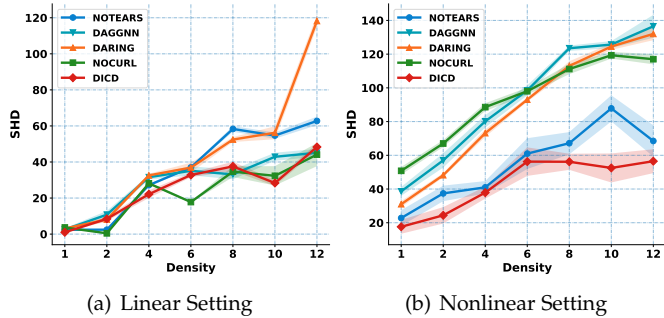


Fig. 4. SHD for different density conditions.

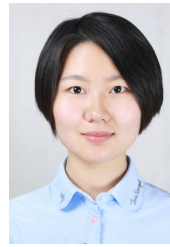
explore the end-to-end causal discovery technique with environment inference, *i.e.*, directly infer partitions of training data without access to environment label. We believe that the idea of this work, *i.e.*, invariant learning inspired causal discovery, provides a potential research direction and will inspire more valuable works for learning identifiable DAG from observation data.

REFERENCES

- [1] X. Zheng, B. Aragam, P. Ravikumar, and E. P. Xing, "Dags with NO TEARS: continuous optimization for structure learning," in *NeurIPS*, 2018, pp. 9492–9503.
- [2] P. Schwab and W. Karlen, "Cxplain: Causal explanations for model interpretation under uncertainty," in *NeurIPS*, 2019, pp. 10 220–10 230.
- [3] M. N. Vu and M. T. Thai, "Pgm-explainer: Probabilistic graphical model explanations for graph neural networks," in *NeurIPS*, 2020.
- [4] K. Sachs, O. Perez, D. Pe'er, D. A. Lauffenburger, and G. P. Nolan, "Causal protein-signaling networks derived from multiparameter single-cell data," *Science*, vol. 308, no. 5721, pp. 523–529, 2005.
- [5] R. Opgen-Rhein and K. Strimmer, "From correlation to causation networks: a simple approximate learning algorithm and its application to high-dimensional plant gene expression data," *BMC systems biology*, vol. 1, no. 1, pp. 1–10, 2007.
- [6] A. D. Sanford and I. A. Moosa, "A bayesian network structure for operational risk modelling in structured finance operations," *JORS*, vol. 63, no. 4, pp. 431–444, 2012.
- [7] Y. Yu, J. Chen, T. Gao, and M. Yu, "DAG-GNN: DAG structure learning with graph neural networks," in *ICML*, vol. 97, 2019, pp. 7154–7163.
- [8] S. Zhu, I. Ng, and Z. Chen, "Causal discovery with reinforcement learning," in *ICLR*, 2020.
- [9] S. Lachapelle, P. Brouillard, T. Deleu, and S. Lacoste-Julien, "Gradient-based neural DAG learning," in *ICLR*. OpenReview.net, 2020.
- [10] X. Zheng, C. Dan, B. Aragam, P. Ravikumar, and E. P. Xing, "Learning sparse nonparametric dags," in *AISTATS*, vol. 108, 2020, pp. 3414–3425.
- [11] R. Bhattacharya, T. Nagarajan, D. Malinsky, and I. Shpitser, "Differentiable causal discovery under unmeasured confounding," in *AISTATS*. PMLR, 2021, pp. 2314–2322.
- [12] Y. Yu and T. Gao, "Dags with no curl: Efficient dag structure learning," in *NeurIPS*, 2020.
- [13] V. Vapnik, "Principles of risk minimization for learning theory," in *NeurIPS*, 1991, pp. 831–838.
- [14] M. Arjovsky, L. Bottou, I. Gulrajani, and D. Lopez-Paz, "Invariant risk minimization," *CoRR*, 2019.
- [15] S. Sagawa, P. W. Koh, T. B. Hashimoto, and P. Liang, "Distributionally robust neural networks for group shifts: On the importance of regularization for worst-case generalization," 2019.
- [16] R. Cadène, C. Dancette, H. Ben-younes, M. Cord, and D. Parikh, "Rubi: Reducing unimodal biases in visual question answering," *CoRR*, vol. abs/1906.10169, 2019.
- [17] D. Krueger, E. Caballero, J. Jacobsen, A. Zhang, J. Binas, D. Zhang, R. L. Priol, and A. C. Courville, "Out-of-distribution generalization via risk extrapolation (rex)," in *ICML*, 2021, pp. 5815–5826.
- [18] Y. He, P. Cui, Z. Shen, R. Xu, F. Liu, and Y. Jiang, "DARING: differentiable causal discovery with residual independence," in *KDD*, 2021, pp. 596–605.
- [19] J. Peters, P. Bühlmann, and N. Meinshausen, "Causal inference by using invariant prediction: identification and confidence intervals," *Journal of the Royal Statistical Society: Series B (Statistical Methodology)*, vol. 78, no. 5, pp. 947–1012, 2016.
- [20] A. Ghassami, N. Kiyavash, B. Huang, and K. Zhang, "Multi-domain causal structure learning in linear systems," in *NeurIPS*, 2018, pp. 6269–6279.
- [21] B. Huang, K. Zhang, J. Zhang, J. D. Ramsey, R. Sanchez-Romero, C. Glymour, and B. Schölkopf, "Causal discovery from heterogeneous/nonstationary data," *JMLR*, vol. 21, pp. 89:1–89:53, 2020.
- [22] A. Ghassami, S. Salehkaleybar, N. Kiyavash, and K. Zhang, "Learning causal structures using regression invariance," in *NIPS*, 2017, pp. 3011–3021.
- [23] B. Huang, K. Zhang, M. Gong, and C. Glymour, "Causal discovery and forecasting in nonstationary environments with state-space models," in *ICML*, 2019, pp. 2901–2910.
- [24] R. Cai, J. Ye, J. Qiao, H. Fu, and Z. Hao, "FOM: fourth-order moment based causal direction identification on the heteroscedastic data," *Neural Networks*, vol. 124, pp. 193–201, 2020.
- [25] J. Qiao, Y. Bai, R. Cai, and Z. Hao, "Causal discovery from multi-domain data using the independence of modularities," *Neural Computing and Applications*, vol. 34, no. 3, pp. 1939–1949, 2022.
- [26] J. Pearl, M. Glymour, and N. P. Jewell, *Causal inference in statistics: A primer*. John Wiley & Sons, 2016.
- [27] G. B. Huang, M. Mattar, T. Berg, and E. Learned-Miller, "Labeled faces in the wild: A database for studying face recognition in unconstrained environments," in *Workshop on faces in Real-Life Images: detection, alignment, and recognition*, 2008.
- [28] J. Deng, W. Dong, R. Socher, L. Li, K. Li, and L. Fei-Fei, "Imagenet: A large-scale hierarchical image database," in *CVPR*, 2009, pp. 248–255.
- [29] P. W. Koh, S. Sagawa, S. M. Xie, M. Zhang, A. Balsubramani, W. Hu, M. Yasunaga, R. L. Phillips, I. Gao, T. Lee *et al.*, "Wilds: A benchmark of in-the-wild distribution shifts," in *ICML*, 2021, pp. 5637–5664.
- [30] P. Bandi, O. Geessink, Q. Manson, M. Van Dijk, M. Balkenhol, M. Hermesen, B. E. Bejnordi, B. Lee, K. Paeng, A. Zhong *et al.*, "From detection of individual metastases to classification of lymph node status at the patient level: the camelyon17 challenge," *TMI*, 2018.
- [31] J. Ni, J. Li, and J. McAuley, "Justifying recommendations using distantly-labeled reviews and fine-grained aspects," in *EMNLP-IJCNLP*, 2019.

- [32] L. Deng, "The mnist database of handwritten digit images for machine learning research," *SPM*, vol. 29, no. 6, pp. 141–142, 2012.
- [33] D. Heckerman, D. Geiger, and D. M. Chickering, "Learning bayesian networks: The combination of knowledge and statistical data," *Maching Learning*, vol. 20, no. 3, pp. 197–243, 1995.
- [34] I. Tsamardinos, L. E. Brown, and C. F. Aliferis, "The max-min hill-climbing bayesian network structure learning algorithm," *Machine learning*, vol. 65, no. 1, pp. 31–78, 2006.
- [35] J. A. Gámez, J. L. Mateo, and J. M. Puerta, "Learning bayesian networks by hill climbing: efficient methods based on progressive restriction of the neighborhood," *Data Mining and Knowledge Discovery*, vol. 22, no. 1-2, pp. 106–148, 2011.
- [36] S. Nie, D. D. Mauá, C. P. de Campos, and Q. Ji, "Advances in learning bayesian networks of bounded treewidth," in *NeurIPS*, 2014, pp. 2285–2293.
- [37] M. Scanagatta, C. P. de Campos, G. Corani, and M. Zaffalon, "Learning bayesian networks with thousands of variables," in *NeurIPS*, 2015, pp. 1864–1872.
- [38] C. Yuan and B. M. Malone, "Learning optimal bayesian networks: A shortest path perspective," *JAIR*, vol. 48, pp. 23–65, 2013.
- [39] H. Manzour, S. Küçükyavuz, and A. Shojaie, "Integer programming for learning directed acyclic graphs from continuous data," *CoRR*, vol. abs/1904.10574, 2019.
- [40] Y. Gao, L. Shen, and S.-T. Xia, "Dag-gan: Causal structure learning with generative adversarial nets," in *ICASSP*. IEEE, 2021, pp. 3320–3324.
- [41] I. Ng, A. Ghassami, and K. Zhang, "On the role of sparsity and DAG constraints for learning linear dags," in *NeurIPS*, 2020.
- [42] D. Wei, T. Gao, and Y. Yu, "Dags with no fears: A closer look at continuous optimization for learning bayesian networks," in *NeurIPS*, 2020.
- [43] G. Varando, "Learning dags without imposing acyclicity," *CoRR*, vol. abs/2006.03005, 2020.
- [44] P. Lippe, T. Cohen, and E. Gavves, "Efficient neural causal discovery without acyclicity constraints," *CoRR*, vol. abs/2107.10483, 2021.
- [45] P. Spirtes, C. N. Glymour, R. Scheines, and D. Heckerman, *Causation, prediction, and search*. MIT press, 2000.
- [46] P. Spirtes, C. Meek, and T. S. Richardson, "Causal inference in the presence of latent variables and selection bias," in *UAI*, 1995, pp. 499–506.
- [47] H. Zhang, K. Zhang, S. Zhou, J. Guan, and J. Zhang, "Testing independence between linear combinations for causal discovery," in *AAAI*, vol. 35, no. 7, 2021, pp. 6538–6546.
- [48] R. Shanmugam, "Causality: Models, reasoning, and inference : Judea pearl; cambridge university press, cambridge, uk, 2000, pp 384, ISBN 0-521-77362-8," *Neurocomputing*, vol. 41, no. 1-4, pp. 189–190, 2001.
- [49] E. Gao, J. Chen, L. Shen, T. Liu, M. Gong, and H. Bondell, "Federated causal discovery," *CoRR*, vol. abs/2112.03555, 2021.
- [50] I. Ng and K. Zhang, "Towards federated bayesian network structure learning with continuous optimization," *CoRR*, vol. abs/2110.09356, 2021.
- [51] R. E. Tillman, D. Danks, and C. Glymour, "Integrating locally learned causal structures with overlapping variables," in *NIPS*. Curran Associates, Inc., 2008, pp. 1665–1672.
- [52] S. Triantafillou, I. Tsamardinos, and I. G. Tollis, "Learning causal structure from overlapping variable sets," in *AISTATS*, ser. JMLR Proceedings, vol. 9. JMLR.org, 2010, pp. 860–867.
- [53] S. Triantafillou and I. Tsamardinos, "Constraint-based causal discovery from multiple interventions over overlapping variable sets," *J. Mach. Learn. Res.*, vol. 16, pp. 2147–2205, 2015.

Yu Wang Yu Wang is currently a first-year PhD student at University of California, San Diego. His research interests lie in Machine Learning and Natural Language Process. During his undergraduate stage in University of Science and Technology of China (USTC), he was awarded Baosteel Scholarship, Huawei Scholarship, Excellent Student Scholarship - Gold, etc.



An Zhang is now a research fellow at National University of Singapore. She received her Ph.D. degree from the Department of Statistics and Applied Probability, National University of Singapore, in 2021. Her areas of interest in research include explainable artificial intelligence, causal representation learning, differentiable causal discovery, and graph neural networks. She has publications appeared in several top conferences such as NeurIPS, ICLR, SIGIR.



Xiang Wang is now a professor at the University of Science and Technology of China (USTC). He received his Ph.D. degree from National University of Singapore in 2019. His research interests include recommender systems, graph learning, and explainable deep learning techniques. He has published some academic papers on international conferences such as NeurIPS, ICLR, KDD, WWW, SIGIR. He serves as a program committee member for several top conferences such as KDD, SIGIR, WWW, and IJCAI, and invited reviewer for prestigious journals such as TKDE, TOIS, TNNLS.



Yancheng Yuan is a research assistant Professor of Department of Applied Mathematics, The Hong Kong Polytechnic University. His research focuses on the optimization theory, algorithm design and software development, mathematical foundation of data science, and data-driven applications. He has published papers in prestigious journals and conferences, including SIOPT, JMLR, IJAA, OMS, ICML, WWW.



Xiangnan He is a professor at the University of Science and Technology of China (USTC). His research interests span information retrieval, data mining, and multi-media analytics. He has over 90 publications in top conferences such as SIGIR, WWW, and MM, KDD, and journals including TKDE, TOIS, and TMM. His work has received the Best Paper Award Honorable Mention in WWW 2018 and SIGIR 2016. He is in the Editorial Board of the AI Open journal, served as the PC chair of CCIS 2019, the area chair of MM 2019, ECML-PKDD 2020, and the (senior) PC member for top conferences including SIGIR, WWW, KDD, WSDM etc.



Tat-Seng Chua is the KITHCT Chair Professor at the School of Computing, National University of Singapore. He was the Acting and Founding Dean of the School during 1998-2000. Dr Chua's main research interest is in multimedia information retrieval and social media analytics. In particular, his research focuses on the extraction, retrieval and question-answering (QA) of text and rich media arising from the Web and multiple social networks. He is the co-Director of NExT, a joint Center between NUS and Tsinghua

University to develop technologies for live social media search. Dr Chua is the 2015 winner of the prestigious ACM SIGMM award for Outstanding Technical Contributions to Multimedia Computing, Communications and Applications. He is the Chair of steering committee of ACM International Conference on Multimedia Retrieval (ICMR) and Multimedia Modeling (MMM) conference series. Dr Chua is also the General Co-Chair of ACM Multimedia 2005, ACM ICMR 2005, ACM SIGIR 2008, and ACM Web Science 2015. He serves in the editorial boards of four international journals. Dr. Chua is the co-Founder of two technology startup companies in Singapore. He holds a PhD from the University of Leeds, UK.

APPENDIX

BASIC STRUCTURE EXAMPLE

In this section, we provide another example shown in Table 8 to demonstrate our motivation introduced in Section 1. In this table, the blue graphs denote the ground truth, while graphs with red edges are the wrong edges in the wrong structures. Below the structures, the first number in front of the parenthesis refers to the least reconstruction loss ($\|\mathbf{X}\mathbf{W} - \mathbf{X}\|_2$) given the structure in the same column of Table 8. Given the structure, we can use the structure to constrain which of the elements in \mathbf{W} should be non-zero elements and others are not. Then we can learn the optimal parameters for these non-zero elements. As shown in the Table, the numbers in the parenthesis refer to the optimal parameters for the edges between A-B, B-C, A-C, respectively. From this table, we can find that with wrong causal structures which have the potential to obtain lower reconstruction loss (*i.e.*, over-reconstruction), the parameters learned given these structures are not consistent across different environments. Thus with the condition given by DICD, we can rule out wrong graphs.

NOTATIONS

We provide the meanings of all the notations used in this paper in Table 9.

PROOF OF THEOREM 4.1

To begin with, we provide the notations used in this proof. We denote the set of all variables as $\{X_1, \dots, X_d\}$, and the vector variable $[X_1, \dots, X_d]^\top$ is denoted as \mathbf{X} in this section. The set of parent nodes of X_i is denoted as $Pa(X_i)$, while the index set of $Pa(X_i)$ is denoted as $Pa(i)$.

First of all, we prove Lemma 4.1 to show that our DICD could yield the true coefficient in linear systems under the true causal structure.

Proof. We consider the linear regression coefficient $\hat{\mathbf{W}}^e$ for every environment e . The regression process in Equation (22) is equivalent to performing the regression for every node $X_m, m \in \{1, \dots, d\}$ from its parents $Pa(X_m)$.

We incorporate the environment information into the expectation operator \mathbb{E}_e . The coefficients of the node X_m is denoted as:

$$[\hat{\mathbf{W}}^e]_m = \arg \min_{\mathbf{w}} \mathbb{E}_e \|\mathbf{X}_m - (\bar{\mathbf{w}} \circ [\mathbf{S}_0]_m)^\top \mathbf{X}\|, \quad (25)$$

where $[\hat{\mathbf{W}}^e]_m$ represents the m -th column of $[\hat{\mathbf{W}}^e]$ and $[\mathbf{S}_0]_m$ is the m -th column of $[\mathbf{S}_0]$. Then we can further express $[\hat{\mathbf{W}}^e]_m$ in Equation (25) as:

$$[\hat{\mathbf{W}}^e]_m = \mathbb{E}_e [\mathbf{X}_m \left(([\mathbf{S}_0]_m \circ \mathbf{X}) ([\mathbf{S}_0]_m \circ \mathbf{X})^\top \right)^{-1} [\mathbf{S}_0]_m \circ \mathbf{X}].$$

For simplicity, we denote $[\mathbf{S}_0]_m \circ \mathbf{X}$ as $\mathbf{X}_{\mathbf{S}_0 m}$.

We extract the m -th column of \mathbf{W}_0 as $[\mathbf{W}_0]_m$, and the true generation process for X_m could be expressed as:

$$X_m = [\mathbf{W}_0]_m^\top \mathbf{X} + z_m, \quad (26)$$

where $z_m \sim \mathcal{N}(0, (\sigma_m^e)^2)$. Then as $[\mathbf{W}_0]$ is the ground truth coefficients, $[\mathbf{W}_0]$ should be consistent with the graph G_0 , as

well as the structure \mathbf{S}_0 . Thus we have: $\mathbf{W}_0 = \mathbf{S}_0 \circ \mathbf{W}_0$, which indicates $[\mathbf{W}_0]_m^\top \mathbf{X} = [\mathbf{S}_0]_m \circ [\mathbf{W}_0]_m^\top \mathbf{X} = [\mathbf{W}_0]_m^\top \mathbf{X}_{\mathbf{S}_0 m}$. Thus the generation process in Equation (26) could be rewritten as:

$$X_m = [\mathbf{W}_0]_m^\top \mathbf{X}_{\mathbf{S}_0 m} + z_m. \quad (27)$$

Then we can substitute Equation (27) into Equation (25) to obtain:

$$[\hat{\mathbf{W}}^e]_m = \mathbb{E}_e [([\mathbf{W}_0]_m^\top \mathbf{X}_{\mathbf{S}_0 m} + z_m)(\mathbf{X}_{\mathbf{S}_0 m}(\mathbf{X}_{\mathbf{S}_0 m})^\top)^{-1} \mathbf{X}_{\mathbf{S}_0 m}].$$

Since z_m is an independent additive noise, we can remove z_m in the above equation and yield:

$$\begin{aligned} [\hat{\mathbf{W}}^e]_m &= \mathbb{E}_e [([\mathbf{w}_0]_m^\top \mathbf{X}_{\mathbf{S}_0 m})(\mathbf{X}_{\mathbf{S}_0 m}(\mathbf{X}_{\mathbf{S}_0 m})^\top)^{-1} \mathbf{X}_{\mathbf{S}_0 m}] \\ &= \mathbb{E}_e [(\mathbf{X}_{\mathbf{S}_0 m}(\mathbf{X}_{\mathbf{S}_0 m})^\top)^{-1} \mathbf{X}_{\mathbf{S}_0 m} \mathbf{X}_{\mathbf{S}_0 m}^\top [\mathbf{W}_0]_m^\top] = [\mathbf{W}_0]_m^\top. \end{aligned} \quad (28)$$

Note that $[\mathbf{W}_0]_m^\top \mathbf{X}_{\mathbf{S}_0 m}$ is a scalar. We adopt the rule $(\mathbf{a} \cdot \mathbf{b})\mathbf{c} = (\mathbf{c} \cdot \mathbf{b}^\top) \cdot \mathbf{a}$, where $\mathbf{a}, \mathbf{b}, \mathbf{c}$ are vectors of the same dimension in the second line. Moreover, since $[\mathbf{W}_0]_m^\top$ is independent of the environment e and the variable vector \mathbf{X} , it can be moved out of the expectation operation.

Based on Equation (28), the obtained coefficients in environment e , $[\hat{\mathbf{W}}^e]_m^\top$, is exactly the true causal coefficients $[\mathbf{W}_0]_m^\top$. Since m is any number in $\{1, \dots, d\}$, we have $\hat{\mathbf{W}}^e = \mathbf{W}_0$. The lemma is proved. \square

With Definition 4.1, we further denote the parents of the variable X_i in G_0 as $Pa_0(X_i)$ and the corresponding indexes as $Pa_0(i)$.

Lemma 4.2 demonstrates that the causal directions between any two variables cannot violate each other in any stable graph and the true causal graph. And we give the proof as following:

Proof. To prove the lemma, we only need to show that given any $X_i \in \{X_1, \dots, X_d\}$ without being the source node, if $\exists X_j$ such that:

$$X_j \in Pa_s(X_i), \quad X_i \in Pre_0(X_j). \quad (29)$$

Then G_s cannot be a stable graph.

To achieve this, we need to incorporate the information of the environment e . Given j satisfying Equation (29), we aim to find j_0 such that:

$$X_{j_0} \in Pa_s(X_i), \quad z_{j_0} \perp Pa_s(X_i) \setminus X_{j_0}.$$

Suppose there exists j satisfying Equation (29), we will find j_0 with the following process:

- (1) Set j_0 to be j ;
- (2) If $\exists X_k \in Pa_s(X_i)$ such that there exists the path from X_{j_0} to X_k , then we set j_0 to be k . In this step, the condition $X_i \in Pre_0(X_{j_0})$ still holds. If there is no such $X_k \in Pa_s(X_i)$ satisfying the above condition, we will exit the iteration.

In this iteration, we always have $X_i \in Pre_0(X_{j_0})$. Also, with the above process, we know that $\forall X_k \in Pa_s(X_i) \setminus \{X_{j_0}\}, X_{j_0} \notin Pre_0(X_k)$, which means:

$$z_{j_0}^e \perp X_k | \forall k \in Pa_s(i) \setminus \{j_0\}. \quad (30)$$

TABLE 8

The specific confounder case in which NOTEARS [1] might make mistakes. Detailed data generation processes are as follows. Environment 1: $A = z_A(\sim \mathcal{N}(0, 4)), B = A/2 + z_B(\sim \mathcal{N}(0, 1)), C = A + B/2 + z_C(\sim \mathcal{N}(0, 4))$. Environment 2: $A = z_A(\sim \mathcal{N}(0, 4)), B = A/2 + z_B(\sim \mathcal{N}(0, 4)), C = A + B/2 + z_C(\sim \mathcal{N}(0, 1))$. Note that only the variance of z_B is different in two environments.

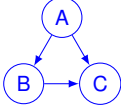
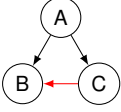
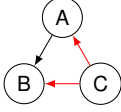
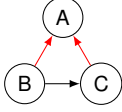
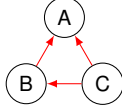
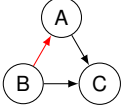
						
e_1	6.00(1.00, 0.50, 0.50)	6.05(0.00, 1.25, 0.40)	8.97(0.00, 0.67, 0.40)	5.67(0.00, 0.67, 1.50)	8.97(0.00, 0.67, 0.40)	5.00(1.00, 1.00, 0.50)
e_2	9.00(1.00, 0.50, 0.50)	8.00(-0.75, 1.25, 1.00)	11.22(-0.75, 0.61, 1.00)	9.96(-0.29, 0.76, 0.90)	11.56(-0.29, 0.76, 0.55)	9.20(0.40, 1.00, 0.50)

TABLE 9
Notations and the corresponding Meanings

Notations	Meanings
n	number of the data samples
d	number of the variables (or nodes)
\mathbf{X}	$\mathbb{R}^{n \times d}$, observational data
\mathbf{x}_j	\mathbb{R}^n , observational data corresponding to the j -th variable
X_j	j -th node variable
F	ground truth structure function
F_j	ground truth structure function corresponding to X_j
f	estimated structure function
f_j	estimated structure function corresponding to X_j
$\text{Pa}(X_j)$	parent set of X_j
$\text{Pa}(j)$	the index set of the parents of X_j
z_j	additive noise of X_j
σ_j^2	variance of z_j
$\mathcal{G}(\cdot)$	corresponding graph of \cdot
\mathbf{W}	$\mathbb{R}^{d \times d}$, the coefficients for all edges of $\mathcal{G}(f)$ in linear situations
m_l	the number of hidden units in the l -th layer in MLP
\mathbf{S}	$\{0, 1\}^{d \times d}$ invariant structure model

Now since the result of the regression from $\text{Pa}_s(X_i)$ to X_i is exactly the m -th column of \mathbf{W}^e , we denote the result of the regression based on Equation (23) as:

$$[\hat{\mathbf{W}}^e]_m = \arg \min_{[w_1, \dots, w_d]^\top} \mathbb{E}_e \|w_{j_0} X_{j_0} + \sum_{k \in \text{Pa}_s(m) \setminus \{j\}} w_k X_k - X_i\|_2^2, \\ \text{s.t. } w_j = 0, \quad j \in \{1, \dots, d\} \setminus \text{Pa}_s(m).$$

Then the optimal value for w_{j_0} is:

$$\hat{w}_{j_0}^e = \frac{\mathbb{E}_e[X_i X_{j_0}] - \sum_{k \in \text{Pa}_s(i) \setminus \{j_0\}} \hat{w}_k^e \mathbb{E}_e[X_k X_{j_0}]}{\mathbb{E}_e[X_{j_0}^2]}. \quad (31)$$

According to the conditions of theorem 4.1, there exist two distinct environments $e_1, e_2 \in \mathcal{E}$ such that $\text{Var}(z_{j_0}^{e_1}) \neq \text{Var}(z_{j_0}^{e_2})$ and for any other node X_i , i.e., $i \neq j_0$, we have $\text{Var}(z_i^{e_1}) = \text{Var}(z_i^{e_2})$.

Hence in the right term in Equation (31), with $X_i \perp z_{j_0}$ (according to the condition $X_i \in \text{Pre}_0(X_{j_0})$), and $\forall k \in \text{Pa}_s(i) \setminus \{j_0\}, z_{j_0}^e \perp X_k$ in Equation (30), we could have:

$$\mathbb{E}_{e_1}[X_i X_{j_0}] = \mathbb{E}_{e_2}[X_i X_{j_0}], \\ \forall k \in \text{Pa}_s(X_i) \setminus \{j_0\}, \mathbb{E}_{e_1}[X_k X_{j_0}] = \mathbb{E}_{e_2}[X_k X_{j_0}].$$

If there exists $k \in \text{Pa}_s(i) \setminus \{j_0\}$ such that \hat{w}_k^e is different across e_1 and e_2 , then G_s is already not stable, which raises the contradiction. Otherwise, if $\hat{w}_k^{e_1} = \hat{w}_k^{e_2}, \forall k \in \text{Pa}_s(i) \setminus \{j_0\}$, then since $\mathbb{E}_{e_1}[X_{j_0}^2] \neq \mathbb{E}_{e_2}[X_{j_0}^2]$, we will have

$$\hat{w}_{j_0}^{e_1} \neq \hat{w}_{j_0}^{e_2}, \quad (32)$$

indicating G_s is not a stable graph. The contradiction still exists.

Thus we can have the conclusion: If G_s is a stable graph, then $\forall X_j \in \text{Pa}_s(X_i)$, we have $X_i \notin \text{Pre}_0(X_j)$. The lemma is proved. \square

Now we give the proof of Theorem 4.2. Since it's written from Theorem 4.1 with Definition 4.1, then Theorem 4.1 will also be proved.

Proof. Note that in this case \mathbf{W}_0 is the optimal parameters for G_0 , and thus it is also the true coefficients for data generation. (as shown in Lemma 4.1.)

To prove Theorem 4.1, we will split the regression loss in Equation (22) to the specific loss value in every environment and every node except source nodes. In other words, we illustrate that for any environment $e \in \mathcal{E}$, $\mathcal{L}^e(\mathbf{S}_0 \circ \mathbf{W}_0) \leq \mathcal{L}^e(\mathbf{S}_s \circ \mathbf{W}_s)$, which could directly lead to Equation (24). Hence, in the following part, with a slight abuse of notation, we will omit the subscript e . We will show that $\forall X_i \in \mathcal{V}$, where \mathcal{V} is the node set, the regression loss from $\text{Pa}(X_i)$ to X_i in G_s is larger or equal than in G_0 , with the equaling condition holds when:

$$i\text{-th column}(\mathbf{W}_0) = i\text{-th column}(\mathbf{W}_s). \quad (33)$$

Given any $X_i \in \mathcal{V}, i \in \{1, \dots, d\}$, we denote all the parents of X_i in G_s, G_0 as $\text{Pa}_s(X_i), \text{Pa}_0(X_i)$ and the corresponding indexes of its parents as $\text{Pa}_s(i), \text{Pa}_0(i)$, respectively. Then the true generation process for the variable X_i could be denoted as:

$$X_i = \sum_{k \in \text{Pa}_0(i)} [\mathbf{W}_0]_{ki} X_k + z_i; \quad z_i \sim \mathcal{N}(0, \sigma_i^2). \quad (34)$$

When performing regression from $\text{Pa}_s(X_i)$ to X_i , we need to constrain $\mathcal{G}(\mathbf{W}_s) = G_s$, which means

$$[\mathbf{W}_s]_{ki} = 0 \forall k \in \{1, \dots, d\} \setminus \text{Pa}_s(i).$$

We denote the minimal loss and the optimal elements as

$$I_i^s = \min_{\{\bar{w}_k | k \in \text{Pa}_s(i)\}} \mathbb{E} \|X_i - \sum_{k \in \text{Pa}_s(i)} \bar{w}_k X_k\|_2^2, \quad (35) \\ \{w_k^* | k \in \text{Pa}_s(i)\} = \arg \min_{\{\bar{w}_k | k \in \text{Pa}_s(i)\}} \mathbb{E} \|X_i - \sum_{k \in \text{Pa}_s(i)} \bar{w}_k X_k\|_2^2,$$

where $\{w_k^* | k \in \text{Pa}_s(i)\}$ is a set and its elements are exactly the corresponding elements of $[\mathbf{W}_s]_i$, i.e., the non-zero elements of i -th column of \mathbf{W}_s .

Then we define three sets of indexes as follows:

$$\begin{aligned}\mathcal{I}_u &= Pa_0(i) \cap Pa_s(i), \\ \mathcal{I}_v &= Pa_0(i) \setminus Pa_s(i), \\ \mathcal{I}_k &= Pa_s(i) \setminus Pa_0(i).\end{aligned}$$

Then after substituting Equation (34) into Equation (35), we have:

$$\begin{aligned}L_i^s &= \min_{\{\bar{w}_k | k \in Pa_s(i)\}} \mathbb{E} \left\| \sum_{u \in \mathcal{I}_u} ([\mathbf{W}_0]_{ui} - \bar{w}_u) X_u \right. \\ &\quad \left. + \sum_{v \in \mathcal{I}_v} [\mathbf{W}_0]_{vi} X_v + \sum_{k \in \mathcal{I}_k} \bar{w}_k X_k + z_i \right\|_2^2.\end{aligned}$$

According to Lemma 4.1, $\forall X_j \in Pa_s(X_i)$, we have $X_i \notin Pre_0(X_j)$, which means $X_j \perp z_i$. Thus we have $z_i \perp Pa_s(X_i)$. By definition, we have $z_i \perp Pa_0(X_i)$, which yield $z_i \perp \{Pa_s(X_i) \cup Pa_0(X_i)\}$. Then we can rewrite the above equation as:

$$\begin{aligned}L_i^s &= \min_{\{\bar{w}_k | k \in Pa_s(i)\}} \mathbb{E} \left\| \sum_{u \in \mathcal{I}_u} ([\mathbf{W}_0]_{ui} - \bar{w}_u) X_u \right. \\ &\quad \left. + \sum_{v \in \mathcal{I}_v} [\mathbf{W}_0]_{vi} X_v + \sum_{k \in \mathcal{I}_k} \bar{w}_k X_k \right\|_2^2 + \sigma_i^2.\end{aligned}$$

Since the reconstruction loss for X_i in the true graph G_0 , denoted as L_i^0 is exactly the variance of the additive noise added on X_i , i.e., σ_i^2 . Thus here we already have $L_i^s \geq L_i^0 = \sigma_i^2$. In the following part, We will explore the conditions that make the equation hold exactly.

Note that $\forall j \in Pa_0(i)$, we have $[\mathbf{W}_0]_{ji} \neq 0$. Then for all the nodes in $\mathcal{I}_u \cup \mathcal{I}_v \cup \mathcal{I}_k$, there must exists a node denoted as $X_{end} \in \mathcal{I}_u \cup \mathcal{I}_v \cup \mathcal{I}_k$ that has no successors in $\mathcal{I}_u \cup \mathcal{I}_v \cup \mathcal{I}_k$ according to G_0 . This means the noises corresponding to X_{end} will be independent from all the other nodes in $\mathcal{I}_u \cup \mathcal{I}_v \cup \mathcal{I}_k$. Then we discuss three situations for X_{end} to be in \mathcal{I}_u , \mathcal{I}_v , and \mathcal{I}_k , respectively:

- If $X_{end} \in \mathcal{I}_u$, we denote the index for X_{end} as u_1 . Then we have:

$$\begin{aligned}L_i^s - L_i^0 &\geq \min_{\{\bar{w}_k | k \in Pa_s(i)\}} \mathbb{E} \left\| \sum_{u \in \mathcal{I}_u \setminus \{u_1\}} ([\mathbf{W}_0]_{ui} - \bar{w}_u) X_u \right. \\ &\quad \left. + \sum_{v \in \mathcal{I}_v} [\mathbf{W}_0]_{vi} X_v + \sum_{k \in \mathcal{I}_k} \bar{w}_k X_k \right\|_2^2 + ([\mathbf{W}_0]_{u_1 i} - \bar{w}_{u_1})^2 \sigma_{u_1}^2.\end{aligned}$$

Then the minimum operation $\min_{\{\bar{w}_k | k \in Pa_s(i)\}}$ in Equation (35) will directly set the optimal value of \bar{w}_{u_1} , i.e., $w_{u_1}^*$ to be $[\mathbf{W}_0]_{u_1 i}$.

- If $X_{end} \in \mathcal{I}_v$, we denote the index for X_{end} as v_1 . Then we have:

$$\begin{aligned}L_i^s - L_i^0 &\geq \min_{\{\bar{w}_k | k \in Pa_s(i)\}} \mathbb{E} \left\| \sum_{u \in \mathcal{I}_u} ([\mathbf{W}_0]_{ui} - \bar{w}_u) X_u \right. \\ &\quad \left. + \sum_{v \in \mathcal{I}_v \setminus \{v_1\}} [\mathbf{W}_0]_{vi} X_v + \sum_{k \in \mathcal{I}_k} \bar{w}_k X_k \right\|_2^2 + [\mathbf{W}_0]_{v_1 i}^2 \sigma_{v_1}^2.\end{aligned}$$

In this case, we will have the strict inequality $L_i^s > L_i^0$, which means the reconstruction loss for G_s will be strictly larger than G_0 .

- If $X_{end} \in \mathcal{I}_k$, we denote the index for X_{end} as k_1 . Then we have:

$$\begin{aligned}L_i^s - L_i^0 &\geq \min_{\{\bar{w}_k | k \in Pa_s(i)\}} \mathbb{E} \left\| \sum_{u \in \mathcal{I}_u} ([\mathbf{W}_0]_{ui} - \bar{w}_u) X_u \right. \\ &\quad \left. + \sum_{v \in \mathcal{I}_v} [\mathbf{W}_0]_{vi} X_v + \sum_{k \in \mathcal{I}_k \setminus \{k_1\}} \bar{w}_k X_k \right\|_2^2 + \bar{w}_{k_1}^2 \sigma_{k_1}^2.\end{aligned}$$

Then the minimum operation $\min_{\{\bar{w}_k | k \in Pa_s(i)\}}$ in Equation (35) will directly set the optimal value of \bar{w}_{k_1} , i.e., $w_{k_1}^*$ to be 0.

If $X_{end} \in \mathcal{I}_v$, then we can already have $L_i^s > L_i^0$. For the other two situations, we will remove $X_{end} \in \mathcal{I}_u$ or \mathcal{I}_k to form the new set \mathcal{I}'_u and \mathcal{I}'_k , then find the new X_{end} in $\mathcal{I}'_u \cup \mathcal{I}_v \cup \mathcal{I}'_k$ to perform the above process again. According to this discussion, we could easily give the necessary and sufficient conditions for L_i^s to be equal to L_i^0 :

- $\mathcal{I}_v = \emptyset$. If not, then there must be one step of removing the current X_{end} such that $X_{end} \in \mathcal{I}_v$, which will directly lead to $L_i^s > L_i^0$.
- $\forall u \in \mathcal{I}_u, w_u^* = [\mathbf{W}_0]_{ui}$.
- $\forall k \in \mathcal{I}_k, w_k^* = 0$.

Now we have the optimal values: $\{w_u | u \in \mathcal{I}_u\}$ and $\{w_k | k \in \mathcal{I}_k\}$. Besides, according to the definition of \mathcal{I}_u and \mathcal{I}_k , and $\mathcal{I}_v = \emptyset$, we have: $\mathcal{I}_u \cup \mathcal{I}_k = Pa_s(j)$ and $\mathcal{I}_u = Pa_0(i)$. Since $\mathcal{I}_k \cap Pa_0(i) = \emptyset$, we have: $\forall k \in \mathcal{I}_k, [\mathbf{W}_0]_{ki} = 0$.

Since the structure of \mathbf{W}_s and \mathbf{W}_0 need to be constrained to be the same as G_s and G_0 , respectively, we must have:

$$[\mathbf{W}_0]_{ji} = [\mathbf{W}_s]_{ji} = 0, \quad \forall j \in \{1, \dots, d\} \setminus (\mathcal{I}_u \cup \mathcal{I}_k).$$

Then according to the above conditions, we have:

$$\text{i-th column}(\mathbf{W}_0) = \text{i-th column}(\mathbf{W}_s).$$

which is Equation (33). Since X_i is any variable except source node in \mathcal{V} , we could have $\mathbf{W}_0 = \mathbf{W}_s$. (Note that for the columns corresponding to the source node, all the elements in these columns should be zero such that $\mathcal{G}(\mathbf{W}_s) = G_s$ and $\mathcal{G}(\mathbf{W}_0) = G_0$).

We conclude the proof of Theorem 4.2. \square